10

Constitutive Equations in Finite Viscoplasticity of Nanocomposite Hydrogels

A.D. Drozdov[1,2,] and J. deClaville Christiansen[2]

[1]Department of Plastics Technology, Danish Technological Institute, Taastrup, Denmark
[2]Department of Mechanical and Manufacturing Engineering, Aalborg University, Aalborg, Denmark
Corresponding author: A.D. Drozdov <add@teknologisk.dk>

10.1 Introduction

This paper deals with constitutive modeling of the viscoplastic response of nanocomposite hydrogels under an arbitrary deformation with finite strains.

Hydrogels are three-dimensional networks of polymer chains connected by physical and chemical cross-links. When a hydrogel is brought in contact with water, it swells retaining its structural integrity and ability to withstand large (up to 3000%) deformations. A shortcoming of conventional (chemically cross-linked) gels that restrains their applicability is that these materials become relatively weak and not sufficiently tough in the swollen state. To enhance mechanical properties of hydrogels without sacrifice of their swellability and extensibility, concentration of reversible physical crosslinks is to be increased [1] either by changes of molecular architecture (double-network hydrogels, gels with hydrophilic and hydrophobic chains [2]) or by reinforcement with nanoparticles that serve as effective multi-functional cross-linkers [3, 4].

Mechanical properties of hydrogels have been a focus of attention in the past decade as these materials demonstrate potential for a wide range of applications including biomedical devices, drug delivery carriers, superabsorbent materials, filters and membranes for selective diffusion, sensors for on-line process monitoring, smart optical systems, and soft actuators [5–8].

Mayuri Prasad and Paolo Di Nardo (Eds.), Innovative Strategies in Tissue Engineering, 135–172.

As mechanical properties of nanocomposite hydrogels are close to those of extracellular matrix (ECM), our interest to their analysis is driven by potential use of these materials for manufacturing synthetic multi-functional scaffolds for *in vitro* support of stem cell culture. The present study focuses on the viscoplastic response of nanocomposite hydrogels in uniaxial tensile cyclic tests. This choice of experimental program is explained by the fact that to ensure survival, proliferation, and differentiation of stem cells imbedded into a hydrogel-based matrix, the latter should be subjected to biophysical cues [9], among which mechanical stimuli play the key role [10, 11]. The standard protocol for mechanical stimulation of stem cells involves periodic deformations with relatively large amplitudes (cyclic loading) followed by periods of rest when thermodynamic equilibrium is established between the hydrogel and its environment [12, 13].

In the past five years, advanced constitutive models for the elastic behavior of hydrogels subjected to swelling have been developed in [14–22], to mention a few. Experimental and theoretical studies of relaxation mechanisms in hydrogels have been performed in [23–26]. Fracture, crack propagation, and self-healing of hydrogels have been investigated in [27–31].

Substantially less attention has been paid to the analysis of irreversible (associated with plastic flow and damage accumulation) phenomena in hydrogels. Stress–strain relations in finite viscoplasticity of hydrogels were developed in [32]. Constitutive equations for the elastic response and damage accumulation in double-network hydrogels were derived in [33, 34]. Time-dependent recovery of residual strains was investigated experimentally in [2, 35, 36].

The objective of this study is threefold: (i) to develop constitutive equations in finite viscoplasticity of nanocomposite hydrogels, (ii) to find adjustable parameters in the stress–strain relations by fitting observations in uniaxial tensile tests with various strain rates and tensile cyclic tests, and (iii) to reveal peculiarities of the mechanical behavior of hydrogels reinforced with various types of nanofiller (silica particles versus clay platelets).

As this work concentrates on the mechanical response of nanocomposite hydrogels swollen in salt-free water, and our aim is to derive relatively simple constitutive equations for their viscoplastic behavior, it seems natural to treat these composite materials as neutral gels and disregard the effects of co- and counter-ions. The novelty of the present approach consists in the following: (i) the initial configuration of a dry undeformed hydrogel is presumed to differ from the reference configuration of an equivalent polymer network (in which stresses in chains vanish), (ii) transformation of the initial

configuration into the reference configuration involves solvent-induced isotropic inflation of the polymer network and its traceless deformation driven by sliding of junctions between chains with respect to their reference positions, (iii) the specific free energy of the polymer network equals the sum of the mechanical energy stored in polymer chains (which depends on the Cauchy–Green tensor for elastic deformation) and the energy of interaction between chains and nanoparticles (which is treated as a function of the Cauchy–Green tensor for plastic deformation).

The exposition is organized as follows. Constitutive equations in finite viscoplasticity of nanocomposite hydrogels under an arbitrary three-dimensional deformation accompanied by swelling are developed in Section 10.2. The governing equations are simplified for uniaxial tension in Section 10.3. Adjustable parameters in the stress–strain relations are determined in Section 10.4 by fitting observations under cyclic deformation. Concluding remarks are formulated in Section 10.5.

10.2 Constitutive Model

To develop constitutive equations for the viscoplastic behavior of a nanocomposite hydrogel that involve a relatively small number of adjustable parameters, a homogenization concept is applied. The solid phase of a nanocomposite hydrogel (formed by a permanent network of flexible chains and a secondary network of clay platelets) is replaced with an equivalent viscoplastic medium whose behavior captures characteristic features of its mechanical response. The presence of nanoparticles within the polymer matrix is accounted for by assuming adjustable parameters in the stress–strain relations to depend on filler content.

10.2.1 Kinematic Relations

Macro-deformation of a nanocomposite hydrogel coincides with that of the equivalent medium. For definiteness, the initial configuration of a hydrogel is chosen to coincide with that of an undeformed dry specimen. Transformation of the initial configuration into the actual configuration is determined by the deformation gradient $\mathbf{F}$. The Cauchy–Green tensors for transition from the initial to actual configuration read

$$\mathbf{B} = \mathbf{F} \cdot \mathbf{F}^{\top}, \qquad \mathbf{C} = \mathbf{F}^{\top} \cdot \mathbf{F}, \tag{10.1}$$

where the dot stands for inner product, and $\top$ denotes transpose. The principal invariants of the Cauchy–Green tensors are denoted as J_1, J_2, J_3.

The reference configuration of the equivalent network (the configuration in which stresses in chain vanish) differs from the initial configuration. Denote by $\mathbf{F}_*$ and $\mathbf{F}_\mathrm{e}$ deformation gradients for transition from the initial configuration into the reference configuration and from the reference configuration into the actual configuration, respectively (the subscript index "e" designates elastic deformation). These tensors are connected with deformation gradient for macro-deformation $\mathbf{F}$ by the multiplicative decomposition formula

$$\mathbf{F} = \mathbf{F}_\mathrm{e} \cdot \mathbf{F}_*. \tag{10.2}$$

Transition from the initial configuration into the reference configuration reflects two processes: (i) changes in specific volume (swelling and shrinkage) induced by solvent transport, and (ii) viscoplastic deformation (sliding of junctions between strands in the equivalent polymer network and slippage of nanoparticles with respect to their positions in the initial configuration).

Local transformation of the initial configuration into the reference configuration due to solvent diffusion is described by the deformation gradient $\mathbf{f}$. For an isotropic equivalent medium,

$$\mathbf{f} = f^{\frac{1}{3}}\mathbf{I}, \tag{10.3}$$

where f stands for the coefficient of inflation induced by solvent uptake, and $\mathbf{I}$ is the unit tensor. Local transformation reflecting irreversible sliding is described by the deformation gradient $\mathbf{F}_\mathrm{p}$ where the subscript index "p" refers to plastic flow. The plastic deformation is presumed to be volume-preserving,

$$\det \mathbf{F}_\mathrm{p} = 1. \tag{10.4}$$

It follows from the multiplicative decomposition formula that [21]

$$\mathbf{F}_* = \mathbf{F}_\mathrm{p} \cdot \mathbf{f}. \tag{10.5}$$

Equations (10.2), (10.3), (10.5) imply that

$$\mathbf{F} = f^{\frac{1}{3}}\mathbf{F}_\mathrm{e} \cdot \mathbf{F}_\mathrm{p}. \tag{10.6}$$

The Cauchy–Green tensors for elastic deformation read

$$\mathbf{B}_\mathrm{e} = \mathbf{F}_\mathrm{e} \cdot \mathbf{F}_\mathrm{e}^\top, \qquad \mathbf{C}_\mathrm{e} = \mathbf{F}_\mathrm{e}^\top \cdot \mathbf{F}_\mathrm{e}. \tag{10.7}$$

To develop differential equations for principal invariants $J_{\mathrm{e}1}$, $J_{\mathrm{e}2}$, $J_{\mathrm{e}3}$ of these tensors, we differentiate Equation (10.6) with respect to time t, introduce velocity gradients

$$\mathbf{L} = \dot{\mathbf{F}} \cdot \mathbf{F}^{-1}, \qquad \mathbf{L}_{\mathrm{e}} = \dot{\mathbf{F}}_{\mathrm{e}} \cdot \mathbf{F}_{\mathrm{e}}^{-1}, \qquad \mathbf{l}_{\mathrm{p}} = \dot{\mathbf{F}}_{\mathrm{p}} \cdot \mathbf{F}_{\mathrm{p}}^{-1}, \tag{10.8}$$

and obtain

$$\mathbf{L} = \mathbf{L}_{\mathrm{e}} + \mathbf{L}_{\mathrm{p}} + \frac{\dot{f}}{3f}\mathbf{I} \tag{10.9}$$

with

$$\mathbf{L}_{\mathrm{p}} = \mathbf{F}_{\mathrm{e}} \cdot \mathbf{l}_{\mathrm{p}} \cdot \mathbf{F}_{\mathrm{e}}^{-1}. \tag{10.10}$$

Equation (10.9) implies that that

$$\mathbf{D} = \mathbf{D}_{\mathrm{e}} + \mathbf{D}_{\mathrm{p}} + \frac{\dot{f}}{3f}\mathbf{I}, \tag{10.11}$$

where

$$\mathbf{D} = \frac{1}{2}(\mathbf{L}+\mathbf{L}^{\top}), \qquad \mathbf{D}_{\mathrm{e}} = \frac{1}{2}(\mathbf{L}_{\mathrm{e}}+\mathbf{L}_{\mathrm{e}}^{\top}), \qquad \mathbf{D}_{\mathrm{p}} = \frac{1}{2}(\mathbf{L}_{\mathrm{p}}+\mathbf{L}_{\mathrm{p}}^{\top}) \tag{10.12}$$

denote rate-of-strain tensors. Under the conventional hypothesis that the plastic spin vanishes,

$$\mathbf{l}_{\mathrm{p}} = \mathbf{l}_{\mathrm{p}}^{\top} = \mathbf{d}_{\mathrm{p}}, \tag{10.13}$$

where $\mathbf{d}_{\mathrm{p}}$ is the rate-of-strain tensor for plastic deformation in the reference configuration, Equations (10.10)–(10.12) imply that

$$2\mathbf{D}_{\mathrm{p}} = \mathbf{F}_{\mathrm{e}} \cdot \mathbf{d}_{\mathrm{p}} \cdot \mathbf{F}_{\mathrm{e}}^{-1} + \mathbf{F}_{\mathrm{e}}^{-\top} \cdot \mathbf{d}_{\mathrm{p}} \cdot \mathbf{F}_{\mathrm{e}}^{\top}. \tag{10.14}$$

Derivatives of the principal invariants of the Cauchy–Green tensors for elastic deformation with respect to time are given by

$$\dot{J}_{\mathrm{e}1} = 2\mathbf{B}_{\mathrm{e}} : \mathbf{D}_{\mathrm{e}}, \quad \dot{J}_{\mathrm{e}2} = 2(J_{\mathrm{e}2}\mathbf{I} - J_{\mathrm{e}3}\mathbf{B}_{\mathrm{e}}^{-1}) : \mathbf{D}_{\mathrm{e}}, \quad \dot{J}_{\mathrm{e}3} = 2J_{\mathrm{e}3}\mathbf{I} : \mathbf{D}_{\mathrm{e}}, \tag{10.15}$$

where the colon stands for convolution of tensors. Combination of Equations (10.11) and (10.15) implies that

$$\begin{aligned}
\dot{J}_{\mathrm{e}1} &= 2\mathbf{B}_{\mathrm{e}} : (\mathbf{D} - \mathbf{D}_{\mathrm{p}}) - \frac{2\dot{f}}{3f}J_{\mathrm{e}1}, \\
\dot{J}_{\mathrm{e}2} &= 2(J_{\mathrm{e}2}\mathbf{I} - J_{\mathrm{e}3}\mathbf{B}_{\mathrm{e}}^{-1}) : (\mathbf{D} - \mathbf{D}_{\mathrm{p}}) - \frac{4\dot{f}}{3f}J_{\mathrm{e}2}, \\
\dot{J}_{\mathrm{e}3} &= 2J_{\mathrm{e}3}\Big[\mathbf{I} : (\mathbf{D} - \mathbf{D}_{\mathrm{p}}) - \frac{\dot{f}}{f}\Big].
\end{aligned} \tag{10.16}$$

It follows from Equations (10.7) and (10.14) that

$$\mathbf{B}_{\mathrm{e}} : \mathbf{D}_{\mathrm{p}} = \mathbf{C}_{\mathrm{e}} : \mathbf{d}_{\mathrm{p}}, \quad \mathbf{I} : \mathbf{D}_{\mathrm{p}} = 0, \quad \mathbf{B}_{\mathrm{e}}^{-1} : \mathbf{D}_{\mathrm{p}} = \mathbf{C}_{\mathrm{e}}^{-1} : \mathbf{d}_{\mathrm{p}}.$$

Insertion of these expressions into Equation (10.16) results in

$$\begin{aligned}
\dot{J}_{\mathrm{e}1} &= 2\mathbf{B}_{\mathrm{e}} : \mathbf{D} - 2\mathbf{C}_{\mathrm{e}} : \mathbf{d}_{\mathrm{p}} - \frac{2\dot{f}}{3f} J_{\mathrm{e}1}, \\
\dot{J}_{\mathrm{e}2} &= -2(\mathbf{B}_{\mathrm{e}}^{-1} : \mathbf{D} - \mathbf{C}_{\mathrm{e}}^{-1} : \mathbf{d}_{\mathrm{p}}) J_{\mathrm{e}3} + 2\Big(\mathbf{I} : \mathbf{D} - \frac{2\dot{f}}{3f}\Big) J_{\mathrm{e}2}, \\
\dot{J}_{\mathrm{e}3} &= 2\Big(\mathbf{I} : \mathbf{D} - \frac{\dot{f}}{f}\Big) J_{\mathrm{e}3}.
\end{aligned} \tag{10.17}$$

Denote by

$$\mathbf{B}_{\mathrm{p}} = \mathbf{F}_{\mathrm{p}} \cdot \mathbf{F}_{\mathrm{p}}^{\top}, \qquad \mathbf{C}_{\mathrm{p}} = \mathbf{F}_{\mathrm{p}}^{\top} \cdot \mathbf{F}_{\mathrm{p}} \tag{10.18}$$

the Cauchy–Green tensors for plastic deformation, and by $J_{\mathrm{p}1}$, $J_{\mathrm{p}2}$, and $J_{\mathrm{p}3} = 1$ their principal invariants. Keeping in mind that $\mathbf{d}_{\mathrm{p}}$ is a traceless tensors, we write, by analogy with Equation (10.17),

$$\dot{J}_{\mathrm{p}1} = 2\mathbf{B}_{\mathrm{p}} : \mathbf{d}_{\mathrm{p}}, \quad \dot{J}_{\mathrm{p}2} = -2\mathbf{B}_{\mathrm{p}}^{-1} : \mathbf{d}_{\mathrm{p}}. \tag{10.19}$$

10.2.2 Free Energy Density of a Hydrogel

Denote by Ψ the specific free energy of a nanocomposite hydrogel (per unit volume in the initial configuration). For a hydrogel with an isotropic polymer network, Ψ is treated as a function of seven arguments

$$\Psi = \Psi(J_{\mathrm{e}1}, J_{\mathrm{e}2}, J_{\mathrm{e}3}, J_{\mathrm{p}1}, J_{\mathrm{p}2}, n, t), \tag{10.20}$$

where n stands for numbers of water molecules per unit volume of a hydrogel in its initial state. An explicit dependence of Ψ on time t is introduced to account for evolution of the equivalent polymer network driven by swelling–shrinkage of a nanocomposite hydrogel. The following equation is adopted for the specific free energy

$$\Psi = \mu_0 n + \Psi_{\mathrm{solid}} + \Psi_{\mathrm{mix}}, \tag{10.21}$$

where μ_0 is chemical potential per solvent molecule in the bath (which, in general, differs from chemical potential μ per solvent molecule in a gel),

$\Psi_{\rm solid}$ denotes strain energy density of the solid phase, $\Psi_{\rm mix}$ stands for the energy of mixing of solvent molecules with chains and nanoparticles in the equivalent network.

The strain energy density of an isotropic equivalent medium reads

$$\Psi_{\rm solid} = \Psi_{\rm solid}(J_{\rm e1}, J_{\rm e2}, J_{\rm e3}, J_{\rm p1}, J_{\rm p2}, t). \tag{10.22}$$

Within the Flory–Huggins theory of mixing, the specific energy of mixing is given by

$$\phi_{\rm s}\Psi_{\rm mix} = \frac{k_B T}{v}(\phi_{\rm f} \ln \phi_{\rm f} + \chi \phi_{\rm s}\phi_{\rm f}), \tag{10.23}$$

where k_B is Boltzmann's constant, T stands for absolute temperature, v is the characteristic volume of a solvent molecule, χ denotes the Flory–Huggins interaction parameter, and

$$\phi_{\rm f} = \frac{nv}{1+nv}, \qquad \phi_{\rm s} = \frac{1}{1+nv} \tag{10.24}$$

are volume fractions of the fluid and solid phases, respectively. Insertion of Equations (10.22) and (10.23) into Equation (10.21) implies that

$$\Psi = \Psi_{\rm solid} + \mu_0 n + \frac{k_B T}{v}\Big(nv \ln \frac{nv}{1+nv} + \chi \frac{nv}{1+nv}\Big). \tag{10.25}$$

10.2.3 Derivation of Constitutive Equations

To develop constitutive equations, we apply the method of [14]: the problem of mechanical deformation of a hydrogel subjected to swelling is immersed in a larger class of problems with volume and surface mass uptake (in terminology of [14], pumps injecting solvent are ascribed to each elementary volume of a specimen).

Under quasi-static deformation of a hydrogel, the first Piola–Kirchhoff stress tensor $\mathbf{P}$ satisfies the equilibrium equations

$$\boldsymbol{\nabla}_0 \cdot \mathbf{P} + \mathbf{b} = \mathbf{0} \qquad (\text{in } \Omega) \qquad \mathbf{n}_0 \cdot \mathbf{P} = \mathbf{t} \qquad (\text{at } \partial\Omega), \tag{10.26}$$

where Ω is an arbitrary domain occupied by the hydrogel in the initial configuration, $\partial\Omega$ is its boundary, $\boldsymbol{\nabla}_0$ is the gradient operator in the initial configuration, $\mathbf{n}_0$ is unit outward normal vector at $\partial\Omega$, $\mathbf{b}$ denotes volume force, and $\mathbf{t}$ is surface traction.

Changes in number of solvent molecules n with time are governed by the equations

$$\frac{\partial n}{\partial t} + \boldsymbol{\nabla}_0 \cdot \mathbf{j}_0 = R \quad (\text{in } \Omega), \qquad \mathbf{n}_0 \cdot \mathbf{j}_0 = -r \quad (\text{at } \partial\Omega). \tag{10.27}$$

Here R is the rate of injection of solvent molecules per unit volume, r is the rate of injection of solvent molecules through unit boundary surface, and $\mathbf{j}_0$ stands for flux of solvent in the initial configuration (number of solvent molecules moving through unit surface per unit time).

Transport of solvent through an isotropic network is described by the diffusion equation

$$\mathbf{j} = -\frac{DN}{k_B T}\boldsymbol{\nabla}\mu, \tag{10.28}$$

where D stands for diffusivity, $N = n/\det \mathbf{F}$ denotes concentration of solvent molecules per unit volume in the actual configuration, and $\mathbf{j}$, $\boldsymbol{\nabla}$ are flux vector and the gradient operator in the actual configuration. Keeping in mind that

$$\mathbf{j}_0 = (\det \mathbf{F})\mathbf{F}^{-1} \cdot \mathbf{j}, \qquad \boldsymbol{\nabla}_0 \mu = \boldsymbol{\nabla}\mu \cdot \mathbf{F},$$

we present Equation (10.28) in the form

$$\mathbf{j}_0 = -\frac{Dn}{k_B T}\mathbf{F}^{-1} \cdot \boldsymbol{\nabla}_0 \mu \cdot \mathbf{F}^{-1}. \tag{10.29}$$

Deformation gradient $\mathbf{F}$ and number of solvent molecules n are connected by the molecular incompressibility condition

$$1 + nv = \det \mathbf{F}, \tag{10.30}$$

which means that volumetric macro-deformation is driven by changes in concentration of solvent molecules.

The free energy imbalance equation is written in the form [14]

$$\frac{\mathrm{d}}{\mathrm{d}t}\int_\Omega \Psi \mathrm{d}V - \Big(\int_\Omega \mathbf{b}\cdot\mathbf{v}\mathrm{d}V + \int_{\partial\Omega} \mathbf{t}\cdot\mathbf{v}\mathrm{d}A\Big) - \Big(\int_\Omega \mu R \mathrm{d}V + \int_{\partial\Omega} \mu r \mathrm{d}A\Big) \leq 0, \tag{10.31}$$

where the term in the first parentheses denotes work of external forces (per unit time), and that in the other parentheses stands for rate of changes in the free energy driven by mass flux. Here $\mathbf{v}$ stands for the velocity vector, $\mathrm{d}V$ is volume element, and $\mathrm{d}A$ is surface element (the volume and surface elements are determined in the initial configuration).

Standard transformations of the expression in the first parentheses in Equation (10.31) (integration by parts with application of Equation (10.26)) result in the formula

$$\int_\Omega \mathbf{b}\cdot\mathbf{v}\mathrm{d}V+\int_{\partial\Omega}\mathbf{t}\cdot\mathbf{v}\mathrm{d}A=\int_\Omega(\det\mathbf{F})\mathbf{T}:\mathbf{D}\mathrm{d}V, \tag{10.32}$$

where $\mathbf{T}$ is the Cauchy stress tensor connected with the Piola–Kirchhoff tensor $\mathbf{P}$ by the equation

$$\mathbf{P}=(\det\mathbf{F})\mathbf{F}^{-1}\cdot\mathbf{T},$$

and $\mathbf{D}$ is given by Equation (10.11).

Calculation of the derivative of free energy density (10.20) with the help of Equations (10.17) and (10.19) implies that

$$\begin{aligned}\frac{\mathrm{d}}{\mathrm{d}t}\int_\Omega\Psi\mathrm{d}V=\int_\Omega\Big\{&\frac{\partial\Psi}{\partial t}+\frac{\partial\Psi}{\partial n}\frac{\partial n}{\partial t}-\frac{2\dot f}{3f}\Big(J_{\mathrm{e}1}\Psi_{,\mathrm{e}1}+2J_{\mathrm{e}2}\Psi_{,\mathrm{e}2}+3J_{\mathrm{e}3}\Psi_{,\mathrm{e}3}\Big)+\\&2\Big[(\Psi_{,\mathrm{e}1}\mathbf{B}_{\mathrm{e}}-J_{\mathrm{e}3}\Psi_{,\mathrm{e}2}\mathbf{B}_{\mathrm{e}}^{-1})+(J_{\mathrm{e}2}\Psi_{,\mathrm{e}2}+J_{\mathrm{e}3}\Psi_{,\mathrm{e}3})\mathbf{I}\Big]:\mathbf{D}+\\&2\Big[(\Psi_{,\mathrm{p}1}\mathbf{B}_{\mathrm{p}}-\Psi_{,\mathrm{p}2}\mathbf{B}_{\mathrm{p}}^{-1})-(\Psi_{,\mathrm{e}1}\mathbf{C}_{\mathrm{e}}-J_{\mathrm{e}3}\Psi_{,\mathrm{e}2}\mathbf{C}_{\mathrm{e}}^{-1})\Big]:\mathbf{d}_{\mathrm{p}}\Big\}\mathrm{d}V,\end{aligned} \tag{10.33}$$

where

$$\Psi_{,em}=\frac{\partial\Psi}{\partial J_{em}}\qquad\Psi_{,\mathrm{p}m}=\frac{\partial\Psi}{\partial J_{\mathrm{p}m}}.$$

The second term in Equation (10.33) is transformed by integration by parts with the help of Equation (10.27),

$$\int_\Omega\frac{\partial\Psi}{\partial n}\frac{\partial n}{\partial t}\mathrm{d}V=\int_\Omega\Big[\frac{\partial\Psi}{\partial n}R+\mathbf{j}_0\cdot\boldsymbol{\nabla}_0\Big(\frac{\partial\Psi}{\partial n}\Big)\Big]\mathrm{d}V+\int_{\partial\Omega}r\frac{\partial\Psi}{\partial n}\mathrm{d}A. \tag{10.34}$$

Combination of Equations (10.33) and (10.34) yields

$$\begin{aligned}&\frac{\mathrm{d}}{\mathrm{d}t}\int_\Omega\Psi\mathrm{d}V\\&\quad=\int_\Omega\Big\{\Theta+2\Big[(\Psi_{,\mathrm{e}1}\mathbf{B}_{\mathrm{e}}-J_{\mathrm{e}3}\Psi_{,\mathrm{e}2}\mathbf{B}_{\mathrm{e}}^{-1})+(J_{\mathrm{e}2}\Psi_{,\mathrm{e}2}+J_{\mathrm{e}3}\Psi_{,\mathrm{e}3})\mathbf{I}\Big]:\mathbf{D}+\\&\qquad2\Big[(\Psi_{,\mathrm{p}1}\mathbf{B}_{\mathrm{p}}-\Psi_{,\mathrm{p}2}\mathbf{B}_{\mathrm{p}}^{-1})-(\Psi_{,\mathrm{e}1}\mathbf{C}_{\mathrm{e}}-J_{\mathrm{e}3}\Psi_{,\mathrm{e}2}\mathbf{C}_{\mathrm{e}}^{-1})\Big]:\mathbf{d}_{\mathrm{p}}+\\&\qquad\Big[\frac{\partial\Psi}{\partial n}R+\mathbf{j}_0\cdot\boldsymbol{\nabla}_0\Big(\frac{\partial\Psi}{\partial n}\Big)\Big]\Big\}\mathrm{d}V+\int_{\partial\Omega}r\frac{\partial\Psi}{\partial n}\mathrm{d}A,\end{aligned} \tag{10.35}$$

where

$$\Theta = \frac{\partial \Psi}{\partial t} - \frac{2\dot{f}}{3f}\Big(J_{\mathrm{e}1}\Psi_{,\mathrm{e}1} + 2J_{\mathrm{e}2}\Psi_{,\mathrm{e}2} + 3J_{\mathrm{e}3}\Psi_{,\mathrm{e}3}\Big). \tag{10.36}$$

The molecular incompressibility condition (10.30) establishes a connection between the deformation gradient $\mathbf{F}$ and the rate of injection of solvent R. To account for this dependence, we differentiate Equation (10.30) with respect to time. Keeping in mind that

$$\frac{\mathrm{d}}{\mathrm{d}t}\det\mathbf{F} = (\det\mathbf{F})\mathbf{I} : \mathbf{D},$$

and replacing the derivative of n by means of Equation (10.27), we obtain

$$v(R - \boldsymbol{\nabla}_0 \cdot \mathbf{j}_0) - (\det\mathbf{F})\mathbf{I} : \mathbf{D} = 0. \tag{10.37}$$

Multiplying Equation (10.37) by an arbitrary function Π, integrating over Ω, and performing integration by parts with the help of Equation (10.28), we arrive at

$$\int_\Omega \Big[\Pi\Big(vR - (\det\mathbf{F})\mathbf{I} : \mathbf{D}\Big) + \mathbf{j}_0 \cdot \boldsymbol{\nabla}_0(\Pi v)\Big]\mathrm{d}V + \int_{\partial\Omega} \Pi v r \mathrm{d}A = 0. \tag{10.38}$$

Inserting Equations (10.32), (10.35) into Equation (10.31) and adding Equation (10.38), we find that

$$\begin{aligned}
&\int_\Omega \Big\{2\Big[(\Psi_{,\mathrm{e}1}\mathbf{B}_\mathrm{e} - J_{\mathrm{e}3}\Psi_{,\mathrm{e}2}\mathbf{B}_\mathrm{e}^{-1}) + (J_{\mathrm{e}2}\Psi_{,\mathrm{e}2} + J_{\mathrm{e}3}\Psi_{,\mathrm{e}3})\mathbf{I} - \\
&\qquad\qquad (\det\mathbf{F})(\mathbf{T} + \Pi\,\mathbf{I})\Big\} : \mathbf{D}\mathrm{d}V + \\
&2\int_\Omega \Big[(\Psi_{,\mathrm{p}1}\mathbf{B}_\mathrm{p} - \Psi_{,\mathrm{p}2}\mathbf{B}_\mathrm{p}^{-1}) - (\Psi_{,\mathrm{e}1}\mathbf{C}_\mathrm{e} - J_{\mathrm{e}3}\Psi_{,\mathrm{e}2}\mathbf{C}_\mathrm{e}^{-1})\Big] : \mathbf{d}_\mathrm{p}\mathrm{d}V + \\
&\int_\Omega \Big(\frac{\partial\Psi}{\partial n} + \Pi v - \mu\Big)R\mathrm{d}V + \int_{\partial\Omega}\Big(\frac{\partial\Psi}{\partial n} + \Pi v - \mu\Big)r\mathrm{d}A + \\
&\int_\Omega \mathbf{j}_0 \cdot \boldsymbol{\nabla}_0\Big(\frac{\partial\Psi}{\partial n} + \Pi v\Big)\mathrm{d}V + \int_\Omega \Theta\mathrm{d}V \le 0.
\end{aligned} \tag{10.39}$$

Keeping in mind that $\mathbf{D}$, R, r are now arbitrary functions (the only connection between them (10.30) is accounted for by means of the function Π), we conclude that the thermodynamic inequality (10.39) is satisfied, provided that (i) the Cauchy stress tensor is given by

$$\mathbf{T} = -\Pi\,\mathbf{I} + \frac{2}{\det\mathbf{F}}\Big[(\Psi_{,\mathrm{e}1}\mathbf{B}_\mathrm{e} - J_{\mathrm{e}3}\Psi_{,\mathrm{e}2}\mathbf{B}_\mathrm{e}^{-1}) + (J_{\mathrm{e}2}\Psi_{,\mathrm{e}2} + J_{\mathrm{e}3}\Psi_{,\mathrm{e}3})\mathbf{I}\Big], \tag{10.40}$$

and (ii) chemical potential reads

$$\mu = \frac{\partial \Psi}{\partial n} + \Pi v. \tag{10.41}$$

It follows from Equations (10.25) and (10.41) that

$$\mu = \mu_0 + \Pi v + k_B T \Big[\ln \frac{nv}{1+nv} + \frac{\chi}{(1+nv)^2} \Big]. \tag{10.42}$$

Substitution of Equations (10.29), (10.40), and (10.41) into Equation (10.39) implies that

$$\int_\Omega \Theta \mathrm{d}V + 2 \int_\Omega \Big[(\Psi_{,\mathrm{p}1} \mathbf{B}_\mathrm{p} - \Psi_{,\mathrm{p}2} \mathbf{B}_\mathrm{p}^{-1}) - (\Psi_{,\mathrm{e}1} \mathbf{C}_\mathrm{e} - J_{\mathrm{e}3} \Psi_{,\mathrm{e}2} \mathbf{C}_\mathrm{e}^{-1}) \Big] : \mathbf{d}_\mathrm{p} \mathrm{d}V -$$
$$\int_\Omega \frac{Dn}{k_B T} \Big(\mathbf{F}^{-1} \cdot \boldsymbol{\nabla}_0 \mu \Big) \cdot \Big(\mathbf{F}^{-1} \cdot \boldsymbol{\nabla}_0 \mu \Big) \mathrm{d}V \le 0. \tag{10.43}$$

Keeping in mind that the last term in Equation (10.43) is non-negative, and using Equations (10.4) and (10.36), we conclude that in order to satisfy the free energy imbalance condition, it suffices to require that (iii) the rate-of-strain tensor for plastic deformation $\mathbf{d}_\mathrm{p}$ is governed by the equation

$$\mathbf{d}_\mathrm{p} = P \Big[(\Psi_{,\mathrm{e}1} \mathbf{C}_\mathrm{e} - J_{\mathrm{e}3} \Psi_{,\mathrm{e}2} \mathbf{C}_\mathrm{e}^{-1}) - (\Psi_{,\mathrm{p}1} \mathbf{B}_\mathrm{p} - \Psi_{,\mathrm{p}2} \mathbf{B}_\mathrm{p}^{-1}) \Big]', \tag{10.44}$$

where P is an arbitrary non-negative function, and the prime stands for the deviatoric component of a tensor, and (iv) the coefficient of inflation of the network f obeys the inequality

$$\frac{\partial \Psi}{\partial t} - \frac{2\dot{f}}{3f} \Big(J_{\mathrm{e}1} \Psi_{,\mathrm{e}1} + 2 J_{\mathrm{e}2} \Psi_{,\mathrm{e}2} + 3 J_{\mathrm{e}3} \Psi_{,\mathrm{e}3} \Big) \le 0. \tag{10.45}$$

It is convenient to present Equation (10.44) in the form

$$\mathbf{d}_\mathrm{p} = P \Big\{ \Big[\Psi_{,\mathrm{e}1} \Big(\mathbf{C}_\mathrm{e} - \frac{1}{3} J_{1\mathrm{e}} \mathbf{I} \Big) - J_{\mathrm{e}3} \Psi_{,\mathrm{e}2} \Big(\mathbf{C}_\mathrm{e}^{-1} - \frac{1}{3} (\mathbf{C}_\mathrm{e}^{-1} : \mathbf{I}) \mathbf{I} \Big) \Big] -$$
$$\Big[\Psi_{,\mathrm{p}1} \Big(\mathbf{B}_\mathrm{p} - \frac{1}{3} J_{1\mathrm{p}} \mathbf{I} \Big) - \Psi_{,\mathrm{p}2} \Big(\mathbf{B}_\mathrm{p}^{-1} - \frac{1}{3} (\mathbf{B}_\mathrm{p}^{-1} : \mathbf{I}) \mathbf{I} \Big) \Big] \Big\}.$$

Taking into account that

$$J_{\mathrm{e}3} (\mathbf{C}_\mathrm{e}^{-1} : \mathbf{I}) = J_{\mathrm{e}2}, \quad \mathbf{B}_\mathrm{p}^{-1} : \mathbf{I} = J_{\mathrm{p}2},$$

we arrive at the formula

$$\mathbf{d}_{\mathrm{p}} = P\Big\{\Big[\Psi_{,\mathrm{e}1}\Big(\mathbf{C}_{\mathrm{e}} - \frac{1}{3}J_{1\mathrm{e}}\mathbf{I}\Big) - \Psi_{,\mathrm{e}2}\Big(J_{\mathrm{e}3}\mathbf{C}_{\mathrm{e}}^{-1} - \frac{1}{3}J_{\mathrm{e}2}\mathbf{I}\Big)\Big] - \Big[\Psi_{,\mathrm{p}1}\Big(\mathbf{B}_{\mathrm{p}} - \frac{1}{3}J_{1\mathrm{p}}\mathbf{I}\Big) - \Psi_{,\mathrm{p}2}\Big(\mathbf{B}_{\mathrm{p}}^{-1} - \frac{1}{3}J_{\mathrm{p}2}\mathbf{I}\Big)\Big]\Big\}. \tag{10.46}$$

It follows from Equations (10.8), (10.13), (10.18) that

$$\dot{\mathbf{B}}_{\mathrm{p}} = \mathbf{d}_{\mathrm{p}} \cdot \mathbf{B}_{\mathrm{p}} + \mathbf{B}_{\mathrm{p}} \cdot \mathbf{d}_{\mathrm{p}}.$$

Substitution of Equation (10.46) into this equation yields

$$\dot{\mathbf{B}}_{\mathrm{p}} = 2P\Big[\frac{1}{2}\Psi_{,\mathrm{e}1}(\mathbf{C}_{\mathrm{e}} \cdot \mathbf{B}_{\mathrm{p}} + \mathbf{B}_{\mathrm{p}} \cdot \mathbf{C}_{\mathrm{e}}) - \frac{1}{2}J_{\mathrm{e}3}\Psi_{,\mathrm{e}2}(\mathbf{C}_{\mathrm{e}}^{-1} \cdot \mathbf{B}_{\mathrm{p}} + \mathbf{B}_{\mathrm{p}} \cdot \mathbf{C}_{\mathrm{e}}^{-1}) - \frac{1}{3}\Big((J_{\mathrm{e}1}\Psi_{,\mathrm{e}1} - J_{\mathrm{e}2}\Psi_{,\mathrm{e}2}) - (J_{\mathrm{p}1}\Psi_{,\mathrm{p}1} - J_{\mathrm{p}2}\Psi_{,\mathrm{p}2})\Big)\mathbf{B}_{\mathrm{p}} + \Psi_{,\mathrm{p}2}\mathbf{I} - \Psi_{,\mathrm{p}1}\mathbf{B}_{\mathrm{p}}^{2}\Big]. \tag{10.47}$$

Equations (10.8)–(10.10) and (10.13) imply that

$$\dot{\mathbf{F}}_{\mathrm{e}} = \Big(\mathbf{L} - \frac{\dot{f}}{3f}\mathbf{I}\Big) \cdot \mathbf{F}_{\mathrm{e}} - \mathbf{F}_{\mathrm{e}} \cdot \mathbf{d}_{\mathrm{p}}.$$

Combination of this equation with Equation (10.37) results in

$$\dot{\mathbf{F}}_{\mathrm{e}} = \Big(\mathbf{L} - \frac{\dot{f}}{3f}\mathbf{I}\Big) \cdot \mathbf{F}_{\mathrm{e}} - P\mathbf{F}_{\mathrm{e}} \cdot \Big\{\Big[\Psi_{,\mathrm{e}1}\Big(\mathbf{C}_{\mathrm{e}} - \frac{1}{3}J_{\mathrm{e}1}\mathbf{I}\Big) - \Psi_{,\mathrm{e}2}\Big(J_{\mathrm{e}3}\mathbf{C}_{\mathrm{e}}^{-1} - \frac{1}{3}J_{\mathrm{e}2}\mathbf{I}\Big)\Big] - \Big[\Psi_{,\mathrm{p}1}\Big(\mathbf{B}_{\mathrm{p}} - \frac{1}{3}J_{\mathrm{p}1}\mathbf{I}\Big) - \Psi_{,\mathrm{p}2}\Big(\mathbf{B}_{\mathrm{p}}^{-1} - \frac{1}{3}J_{\mathrm{p}2}\mathbf{I}\Big)\Big]\Big\}. \tag{10.48}$$

Given a free energy density (10.20), Equations (10.40), (10.41), (10.47), (10.48) provide stress–strain relations in finite viscoplasticity of hydrogels.

10.3 Simplification of the Constitutive Equations

Our aim now is to perform quantitative investigation of the viscoplastic response of nanocomposite hydrogels in short-term tests whose duration is noticeably lower than the characteristic time for diffusion of solvent. For

this purpose, we simplify the constitutive equations in order (i) to make them suitable for fitting experimental data and (ii) to reduce the number of adjustable parameters.

First, we suppose that the strain energy density $\Psi_{\rm solid}$ depends on principal invariants $J_{\rm e1}$, $J_{\rm e3}$, and $J_{\rm p1}$ only, and present this function in the form

$$\Psi_{\rm solid} = W_1(J_{\rm e1}, J_{\rm e3}, t) + W_2(J_{\rm p1}, t), \tag{10.49}$$

where W_1 denotes mechanical energy stored in individual chains of the equivalent polymer network (this quantity depends on principal invariants of the Cauchy–Green tensor for elastic deformation) and W_2 stands for the energy of interaction between chains and nanoparticles (treated as a function of principal invariants of the Cauchy–Green tensor for plastic deformation). The influence of second principal invariants of the corresponding Cauchy–Green tensors on the mechanical response is disregarded in Equation (10.49).

Substitution of Equations (10.21), (10.24), (10.30), (10.49) into Equation (10.40) implies that

$$\mathbf{T} = -\Pi\,\mathbf{I} + 2\phi_{\rm s}(w_1\mathbf{B}_{\rm e} + J_{\rm e3}w_1'\mathbf{I}), \tag{10.50}$$

where

$$w_1 = \frac{\partial W_1}{\partial J_{\rm e1}}, \qquad w_1' = \frac{\partial W_1}{\partial J_{\rm e3}}. \tag{10.51}$$

Combination of Equations (10.47–10.49) results in

$$\begin{aligned}
\dot{\mathbf{B}}_{\rm p} &= 2P\Big[\frac{1}{2}w_1(\mathbf{C}_{\rm e}\cdot\mathbf{B}_{\rm p} + \mathbf{B}_{\rm p}\cdot\mathbf{C}_{\rm e}) - \frac{1}{3}(w_1 J_{\rm e1} - w_2 J_{\rm p1})\mathbf{B}_{\rm p} - w_2\mathbf{B}_{\rm p}^2\Big],\\
\dot{\mathbf{F}}_{\rm e} &= \Big(\mathbf{L} - \frac{\dot f}{3f}\mathbf{I}\Big)\cdot\mathbf{F}_{\rm e} - P\mathbf{F}_{\rm e}\cdot\Big[w_1\Big(\mathbf{C}_{\rm e} - \frac{1}{3}J_{\rm e1}\mathbf{I}\Big) -\\
&\qquad\qquad w_2\Big(\mathbf{B}_{\rm p} - \frac{1}{3}J_{\rm p1}\mathbf{I}\Big)\Big]
\end{aligned} \tag{10.52}$$

with

$$w_2 = \frac{\partial W_2}{\partial J_{\rm p1}}. \tag{10.53}$$

Under an arbitrary deformation of a nanocomposite hydrogel subjected to swelling, Equations (10.50)–(10.52) together with Equation (10.42) for chemical potential should be accompanied by the equilibrium equations for the Cauchy stress tensor $\mathbf{T}$ and diffusion Equation (10.27) with $R = 0$,

$$\dot n = \boldsymbol{\nabla}_0\cdot\Big(\frac{Dn}{k_BT}\mathbf{F}^{-1}\cdot\boldsymbol{\nabla}_0\mu\cdot\mathbf{F}^{-1}\Big).$$

In conventional mechanical tests, a hydrogel specimen is, first, swollen in water (to reach a fixed degree of swelling), then annealed without contact with water bath (to reach an homogeneous distribution of solvent across the sample), and, afterwards, loaded with a relatively high strain rate (to avoid evaporation of solvent from the surface). After annealing, concentration of solvent molecules becomes independent of spatial coordinates, but its value differs from that in a fully swollen sample (chemical potential μ does not coincide with μ_0). When the characteristic time for diffusion of solvent exceeds substantially duration of a test, changes in n under deformation can be neglected, and this quantity may be treated as an experimental parameter. Keeping in mind that n remains constant, we disregard dependencies of W_1, W_2 and f on time. Adjustable parameters in expressions for W_1, W_2, f adopt, however, different values for different concentrations of solvent n.

Introducing the notation $p = \Pi - 2\phi_{\rm s} J_{\rm e3} w_1'$ and setting $\dot{f} = 0$ in Equation (10.52), we present Equations (10.50) and (10.52) in the form

$$\begin{aligned}
\mathbf{T} &= -p\mathbf{I} + 2\phi_{\rm s} w_1 \mathbf{B}_{\rm e},\\
\dot{\mathbf{B}}_{\rm p} &= 2P\Big[\frac{1}{2} w_1 (\mathbf{C}_{\rm e}\cdot\mathbf{B}_{\rm p} + \mathbf{B}_{\rm p}\cdot\mathbf{C}_{\rm e}) - \frac{1}{3}(w_1 J_{\rm e1} - w_2 J_{\rm p1})\mathbf{B}_{\rm p} - w_2 \mathbf{B}_{\rm p}^2\Big],\\
\dot{\mathbf{F}}_{\rm e} &= \mathbf{L}\cdot\mathbf{F}_{\rm e} - P\mathbf{F}_{\rm e}\cdot\Big[w_1\Big(\mathbf{C}_{\rm e} - \frac{1}{3}J_{\rm e1}\mathbf{I}\Big) - w_2\Big(\mathbf{B}_{\rm p} - \frac{1}{3}J_{\rm p1}\mathbf{I}\Big)\Big]. \quad (10.54)
\end{aligned}$$

The deformation gradient $\mathbf{F}$ is split into the product of the deformation gradient driven by swelling from the dry state into the undeformed swollen state $(1+nv)^{\frac{1}{3}}\mathbf{I}$ and the loading-induced deformation gradient $\tilde{\mathbf{F}}$,

$$\mathbf{F} = \tilde{\mathbf{F}}(1+nv)^{\frac{1}{3}}. \quad (10.55)$$

Combination of Equations (10.6) and (10.55) implies that

$$\mathbf{F}_{\rm e} = \Big(\frac{1+nv}{f}\Big)^{\frac{1}{3}}\tilde{\mathbf{F}}\cdot\mathbf{F}_{\rm p}^{-1}. \quad (10.56)$$

Under uniaxial deformation of an incompressible medium, tensor $\tilde{\mathbf{F}}$ reads

$$\tilde{\mathbf{F}} = k\mathbf{e}_1\mathbf{e}_1 + k^{-\frac{1}{2}}(\mathbf{e}_2\mathbf{e}_2 + \mathbf{e}_3\mathbf{e}_3), \quad (10.57)$$

where $\mathbf{e}_m$ $(m = 1,2,3)$ are base vectors of a Cartesian frame in the initial state, and k stands for elongation ratio. Assuming tensor $\mathbf{F}_{\rm p}$ to be determined by Equation (10.57) with a coefficient $k_{\rm p}$, we find from Equation (10.56) that

$$\mathbf{F}_{\rm e} = \Big(\frac{1+nv}{f}\Big)^{\frac{1}{3}}\Big[\frac{k}{k_{\rm p}}\mathbf{e}_1\mathbf{e}_1 + \Big(\frac{k_{\rm p}}{k}\Big)^{\frac{1}{2}}(\mathbf{e}_2\mathbf{e}_2 + \mathbf{e}_3\mathbf{e}_3)\Big]. \quad (10.58)$$

Insertion of Equations (10.57) and (10.58) into Equation (10.54) results in

$$\dot{k}_{\mathrm{p}} = \frac{2}{3}P\Big[w_1 X\frac{k^3 - k_{\mathrm{p}}^3}{kk_{\mathrm{p}}} - w_2(k_{\mathrm{p}}^3 - 1)\Big] \tag{10.59}$$

with

$$X = \Big(\frac{1+nv}{f}\Big)^{\frac{2}{3}}. \tag{10.60}$$

Keeping in mind that under uniaxial tension, the stress tensor is given by

$$\mathbf{T} = \sigma k\mathbf{e}_1\mathbf{e}_1,$$

where σ stands for engineering tensile stress, we find from Equation (10.54) that

$$\sigma = 2\phi_{\mathrm{s}}w_1 X\frac{k^3 - k_{\mathrm{p}}^3}{k^2k_{\mathrm{p}}^2}. \tag{10.61}$$

Constitutive equations for uniaxial tension of hydrogels (10.59), (10.61) involve two functions, w_1 and w_2, that characterize the energy stored in polymer chains and the energy of inter-chain interactions.

The following expression is adopted for the strain energy density of the equivalent polymer network [37]

$$W_1 = -\frac{1}{2}G\Big[J\ln\Big(1 - \frac{J_{\mathrm{e1}} - 3}{J}\Big) + \frac{1}{2}\ln J_{\mathrm{e3}}\Big], \tag{10.62}$$

where G stands for an elastic modulus, and $J > 0$ characterizes extensibility of chains. When $J \to \infty$, Equation (10.62) is transformed into the specific strain energy of a network of flexible chains [38]

$$\Psi_{\mathrm{solid}} = \frac{1}{2}G\Big[(J_{\mathrm{e1}} - 3) - \frac{1}{2}\ln J_{\mathrm{e3}}\Big].$$

Differentiation of Equation (10.62) with respect to J_{e1} implies that

$$w_1 = \frac{1}{2}G\Big(1 - \frac{J_{\mathrm{e1}} - 3}{J}\Big)^{-1}. \tag{10.63}$$

The energy of inter-chain interaction W_2 is determined by integration of Equation (10.53) with

$$w_2 = \frac{1}{2}\tilde{G}\Big[1 + K(J_{\mathrm{p1}} - 3)^{\alpha}\Big], \tag{10.64}$$

where $\tilde{G}$ stands for an analog of elastic modulus, and $K > 0$, α are material constants. To reduce the number of adjustable parameters, we presume that

$$K = 1, \qquad \alpha = 2$$

under tension, and

$$\alpha = -\frac{1}{2}$$

under retraction.

Insertion of Equations (10.63) and (10.64) into Equations (10.59) and (10.61) results in the stress–strain relation

$$\sigma = GX\phi_{\rm s}\Big[1 - \frac{1}{J}\Big(X\Big(\frac{k^2}{k_{\rm p}^2} + 2\frac{k_{\rm p}}{k}\Big) - 3\Big)\Big]^{-1}\frac{k^3 - k_{\rm p}^3}{k^2 k_{\rm p}^2} \tag{10.65}$$

and the kinetic equation for plastic flow

$$\dot{k}_{\rm p} = S\Big\{X\Big[1 - \frac{1}{J}\Big(X\Big(\frac{k^2}{k_{\rm p}^2} + 2\frac{k_{\rm p}}{k}\Big) - 3\Big)\Big]^{-1}\frac{k^3 - k_{\rm p}^3}{kk_{\rm p}} - R\Big[1 + K\Big(k_{\rm p}^2 + \frac{2}{k_{\rm p}} - 3\Big)^{\alpha}\Big](k_{\rm p}^3 - 1)\Big\}\frac{|\dot{k}|}{k} \tag{10.66}$$

with

$$S = \frac{PG}{3D}, \qquad R = \frac{\tilde{G}}{G}, \tag{10.67}$$

where $D = |\dot{k}|/k$ stands for strain-rate intensity.

Constitutive Equations (10.65) and (10.66) involve six adjustable parameters: (i) G stands for elastic modulus of an equivalent polymer network, (ii) X characterizes swelling-induced inflation of the network, (iii) J is a measure of extensibility of chains, (iv) S denotes rate of plastic flow, (v) R stands for strength of inter-chain interactions, (vi) K characterizes energy of inter-chain interactions under retraction. These quantities may be affected by composition of a hydrogel, strain rate $\dot{k}$ (due to the neglect of viscoelastic properties associated with rearrangement of polymer network), and deformation program (the energy of interaction W_2 adopts different values under tension and retraction).

Although the number of material constants in the constitutive equations appears to be reasonable compared with conventional models in finite viscoplasticity of polymers, this number can be reduced further for special loading

programs. In particular, when observations are analyzed on as-prepared hydrogels, one can set

$$X = 1, \tag{10.68}$$

which means that the reference state of the equivalent polymer network coincides with the as-prepared state.

In the analysis of active (without unloading) deformations of as-prepared hydrogels, the dimensionless parameter K is not needed, which implies that the total number of parameters to be found by matching observations is reduced to four.

10.4 Fitting of Observations

We intend now to determine adjustable parameters in the stress–strain relations by fitting experimental data on nanocomposite hydrogels under uniaxial tension with finite strains and to assess the effects of type and content of nanofiller on the kinetics of plastic flow. Approximation of experimental stress–strain diagrams is performed for hydrogels with poly(dimethylacrylamide) and polyacrylamide matrices. Hydrogel specimens are characterized by polymer content $\phi_{\rm p} = m_{\rm polymer}/m_{\rm water}$, nanofiller content $\phi_{\rm f} = m_{\rm filler}/m_{\rm water}$, concentration of solid phase $\phi_{\rm s} = (m_{\rm polymer} + m_{\rm filler})/(m_{\rm polymer} + m_{\rm filler} + m_{\rm water})$, where $m_{\rm polymer}$, $m_{\rm filler}$, $m_{\rm water}$ are masses of monomers, filler particles, and water in the as-prepared state, and degree of swelling $Q = M_{\rm water}/(m_{\rm polymer} + m_{\rm filler})$, where $M_{\rm water}$ stands for mass of solvent in the actual state.

10.4.1 Nanocomposite Hydrogels Subjected to Drying and Swelling

To demonstrate the role of coefficient of inflation f in constitutive modeling, we focus on the analysis of mechanical response of nanocomposite hydrogels subjected to drying and subsequent swelling.

We begin with observations on poly (N,N-dimethylacrylamide) (DMAA) physical gels reinforced with Laponite XLG nanoclay (NC). Samples are prepared by free-radical polymerization of N,N-dimethylacrylamide (DMAA) in an aqueous dispersion of nanoclay by using potassium peroxydisulfate $K_2S_2O_8$ (KPS) as an initiator and tetramethylethylenediamine (TEMED) as a catalyst [39].

The experimental procedure involved: (i) drying of as-prepared samples (with $\phi_{\rm p} = 99$ g/L, $\phi_{\rm f} = 25.4$ g/L, and $Q = 7.2$) down to various degrees of swelling $Q_{\rm dry}$ (in the range between 0.06 and 3.0), (ii) re-swelling of

dried samples to the initial degree of swelling Q, (iii) uniaxial tensile tests on dried–reswollen specimens. Mechanical tests were performed at room temperature with strain rate $\dot{\epsilon} = 0.02\,\mathrm{s}^{-1}$ ($\epsilon = k - 1$ stands for engineering tensile strain) up to breakage of samples.

Experimental stress–strain diagrams are depicted in Figure 10.1 where engineering stress σ is plotted versus elongation ratio k. To reduce the number of material constants to be found by matching observations, we presume the response of the nanocomposite hydrogels to be merely elastic. By setting $S = 0$ in Equation (10.66), we conclude that $k_{\mathrm{p}} = 1$ and each stress–strain curve is determined by three parameters G, J, X.

We begin with fitting observations on the as-prepared specimen for which Equation (10.68) is fulfilled. To find adjustable parameters G and J, we fix some interval $[0, J^{\circ}]$, where J is located, and divide this interval into $I = 10$ sub-intervals by the points $J^{(i)} = i\Delta J$ with $\Delta J = J^{\circ}/I$ ($i = 0, 1, \ldots, I-1$). For each $J^{(i)}$, Equations (10.65), (10.66) are integrated numerically by the Runge–Kutta method with step $\Delta t = 0.01$. The modulus G is calculated by the least-squares technique from the condition of minimum of the function

$$F = \sum_{n} \Big[\sigma^{\mathrm{exp}}(k_n) - \sigma^{\mathrm{num}}(k_n)\Big]^2,$$

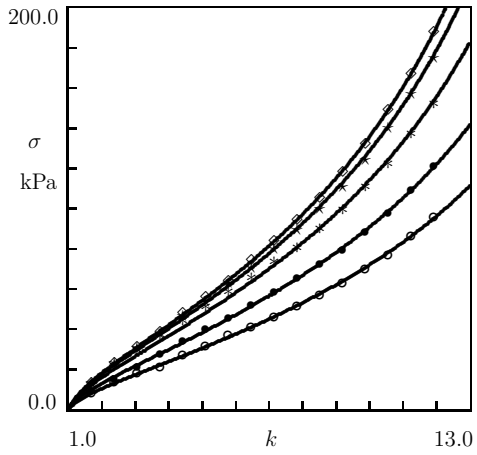

Figure 10.1 Stress σ versus elongation ratio k. Symbols: experimental data in tensile tests on DMAA-NC hydrogel subjected to drying down to various Q_{dry} and subsequent re-swelling up to $Q = 7.2$ ($\circ$ – as-prepared; $\bullet$ – $Q_{\mathrm{dry}} = 3.0$; $*$ – $Q_{\mathrm{dry}} = 1.7$; $\star$ – $Q_{\mathrm{dry}} = 0.8$; $\diamond$ – $Q_{\mathrm{dry}} = 0.06$). Solid lines: results of simulation.

where summation is performed over all elongation ratios k_n at which the observations are reported, $\sigma^{\rm exp}$ stands for engineering stress measured in the test, and $\sigma^{\rm num}$ is given by Equation (10.65). The best-fit value of J is found from the condition of minimum of F. Afterwards, the initial interval is replaced with new interval $[J - \Delta J, J + \Delta J]$, and the calculations are repeated.

After finding the best-fit value $G = 48.2$ kPa, we fix this quantity, and match observations on samples subjected to drying-reswelling by means of the above algorithm with adjustable parameters X and J. Given X, we calculate f from Equation (10.60) and plot f and J versus $Q_{\rm dry}$ in Figure 10.2. The data are approximated by the linear equations

$$f = f_0 + f_1 Q_{\rm dry}, \qquad J = J_0 + J_1 Q_{\rm dry} \tag{10.69}$$

with coefficients calculated by the least-squares technique. Following [39], the strong (by twice) reduction in f induced by drying and re-swelling is attributed to rearrangement of the secondary network (a house-of-cards structure formed by clay platelets).

10.4.2 As-Prepared Poly(Dimethylacrylamide)–Silica Hydrogels

We proceed with the analysis of observations on polydimethylacrylamide–silica (DMAA-Si) hydrogels manufactured by free-radical polymerization of N,N-dimethylacrylamide in aqueous suspensions of silica nanoparticles

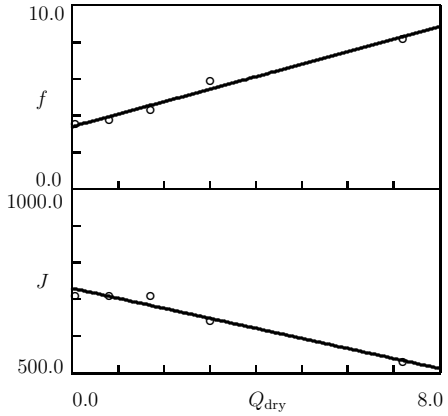

Figure 10.2 Parameters f and J versus solvent content after drying $Q_{\rm dry}$. Circles: treatment of observations on DMAA-NC hydrogels. Solid lines: approximation of the data by Equation (10.69).

(Si) by using KPS and TEMED as initiator and catalyst, respectively [40].

First, experimental data are matched in tensile tests with strain rate $\dot{\epsilon} = 0.06\ \mathrm{s}^{-1}$ at room temperature on as-prepared specimens with a fixed concentration of polymer network $\phi_{\mathrm{p}} = 142.2$ g/L and concentrations of nanoparticles ϕ_{f} ranging from 71.4 to 710.5 g/L (Figure 10.3). According to Equation (10.68), their viscoplastic response is determined by four adjustable parameters G, J, R, S.

To find these quantities, we start with fitting observations on a specimen with $\phi_{\mathrm{f}} = 710.5$ g/L by using the above algorithm. After finding the best-fit values $J = 28.0$ and $S = 1.7$, we fix these quantities and approximate experimental data on samples with $\phi_{\mathrm{f}} = 71.4$, 142.7, and 284.4 g/L with the help of two parameters G, R.

The influence of concentration of solid phase on elastic moduli G and $\tilde{G}$ (given R, the latter is determined from Equation (10.67)) is illustrated in Figure 10.4 where these quantities are plotted versus ϕ_{s}. The data are approximated by the equations

$$G = G_0 + G_1\phi_{\mathrm{s}}, \qquad \tilde{G} = \tilde{G}_0 \tag{10.70}$$

with coefficients calculated by the least-squares technique. Figure 10.4 shows that G grows with concentration of silica particles, in agreement with

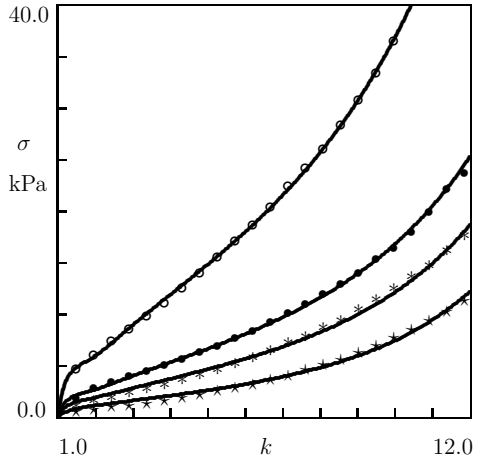

Figure 10.3 Stress σ versus elongation ratio k. Symbols: experimental data in tensile tests on DMAA-Si hydrogels with $\phi_{\mathrm{p}} = 142$ g/L and various ϕ_{f} g/L ($\circ$ – 710.5; $\bullet$ – 284.4; $*$ – 142.7; $\star$ – 71.4). Solid lines: results of simulation.

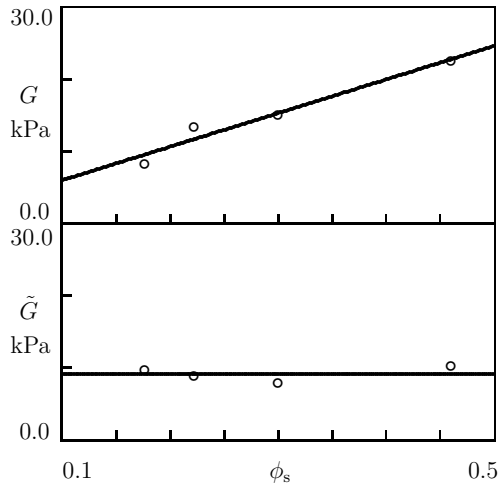

Figure 10.4 Parameters G and $\tilde{G}$ versus concentration of solid phase ϕ_s. Circles: treatment of observations in tensile tests on DMAA-Si hydrogels with $\phi_p = 142$ g/L and various ϕ_f g/L. Solid lines: approximation of the data by Equation (10.70).

observations on other nanocomposite hydrogels [35], whereas $\tilde{G}$ remains constant.

To assess plastic flow in nanocomposite hydrogels under tension, simulation of the stress–strain relations is conducted. Results of numerical analysis are reported in Figure 10.5. According to this figure, (i) nanocomposite hydrogels reveal pronounced plastic deformation (with plastic strains exceeding 100%), and (ii) elongation ratio for plastic deformation k_p decreases weakly with concentration of nanoparticles.

To evaluate the effect of strain rate on the mechanical response of nanocomposite hydrogels, observations are matched on specimens with a fixed concentration of polymer network $\phi_p = 142.2$ g/L and concentrations of nanoparticles $\phi_f = 142.7$ and $\phi_f = 710.5$ g/L under tension with strain rates $\dot{\epsilon} = 0.06$ and 0.6 s^{-1}. Experimental data are depicted in Figure 10.6. Adjustable parameters are found by approximation of the experimental data with the help of the above algorithm. Each set of observations is fitted separately with the help of two parameters G, R. The best-fit value of J and the values of S and R at strain rate $\dot{\epsilon} = 0.06$ s^{-1} are taken from Figure 10.4. The value of S at $\dot{\epsilon} = 0.6$ s^{-1} is calculated from Equation (10.67), whereas the value of R at this strain rate is determined by matching the stress–strain diagrams.

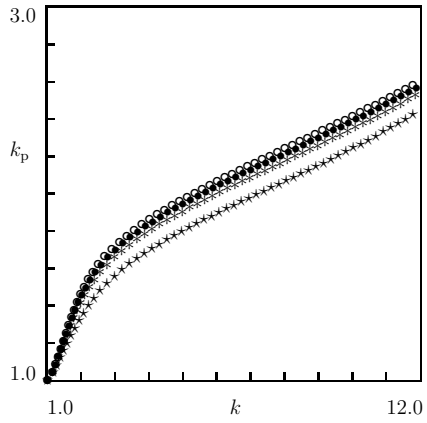

Figure 10.5 Elongation ratio for plastic deformation $k_{\rm p}$ versus elongation ratio k. Symbols: results of simulation for tensile tests on DMAA-Si hydrogels with $\phi_{\rm p} = 142$ g/L and various $\phi_{\rm f}$ g/L ($\circ$ – 710.5; $\bullet$ – 284.4; $*$ – 142.7; $\star$ – 71.4).

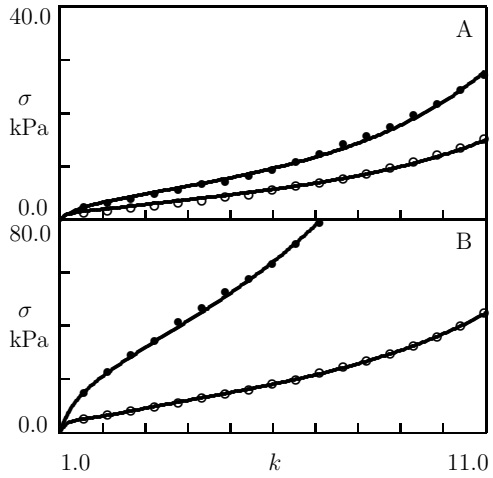

Figure 10.6 Stress σ versus elongation ratio k. Symbols: experimental data in tensile tests with various strain rates $\dot\epsilon$ s^{-1} ($\circ$ – 0.06; $\bullet$ – 0.6) on DMAA-Si hydrogels with $\phi_{\rm p} = 142.2$ g/L and $\phi_{\rm f} = 142.7$ g/L (A), $\phi_{\rm f} = 710.5$ g/L (B). Solid lines: results of simulation.

Evolution of elastic moduli with strain rate $\dot\epsilon$ is illustrated in Figure 10.7 where G and $\tilde G$ are depicted versus duration of loading $t' = (k_{\max} - 1)/\dot\epsilon$ with $k_{\max} = 11$. For comparison, observations in tensile relaxation tests with strain $\epsilon = 0.5$ are also presented (in semi-logarithmic coordinates with $\log = \log_{10}$). Following [40], relaxation curves are plotted in the form $\tilde\sigma(t')$

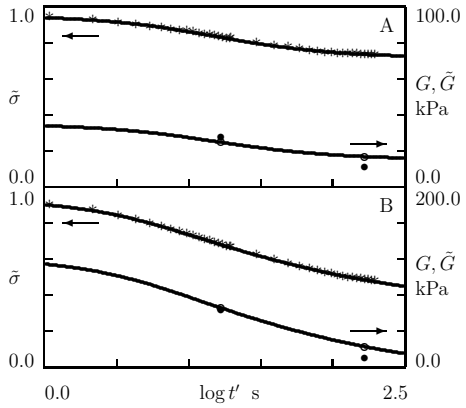

Figure 10.7 Dimensionless stress $\tilde{\sigma}$ ($*$) versus relaxation time t' and moduli G ($\circ$), $\tilde{G}$ ($\bullet$) versus loading time t'. Symbols: observations on DMAA-Si hydrogels with $\phi_{\rm n} = 142.2$ g/L, $\phi_{\rm f} = 142.7$ g/L (A), and $\phi_{\rm f} = 710.5$ g/L (B). Asterisks: experimental data in tensile relaxation test with strain $\epsilon = 0.5$. Circles: treatment of experimental data in tensile tests with strain rates $\dot{\epsilon} = 0.06$ and 0.6 $\rm s^{-1}$. Solid lines: results of simulation.

with $\tilde{\sigma} = \sigma/\sigma_0$ and $t' = t - t_0$, where t_0 and σ_0 stand for time and stress at the beginning of relaxation. The aim of Figure 10.7 (where observations in relaxation tests are approximated with a model proposed in [41]) is to demonstrate that alteration of elastic modulus G with strain rate found by fitting observations in tensile tests may be ascribed to the viscoelastic response of nanocomposite hydrogels (treated as rearrangement of chains in a transient network). The latter is disregarded in the constitutive model as its account leads to a substantial increase in the number of adjustable parameters.

To examine the influence of nanofiller on the viscoplastic behavior of DMAA-Si hydrogels under tensile cyclic deformation, we analyze observations reported in Figure 10.8. The experimental stress–strain diagrams are obtained on as-prepared specimens (with a fixed concentration of polymer network $\phi_{\rm p} = 142.2$ g/L and various concentrations of nanoparticles $\phi_{\rm f} = 142.7$, 284.4, 710.5 g/L) subjected to tension with a constant strain rate $\dot{\epsilon} = 0.06$ $\rm s^{-1}$ up to maximum elongation ratio $k_{\max} = 6$ and retraction down to the zero minimum stress $\sigma_{\min} = 0$.

As the stress–strain curves under tension reported in Figure 10.8 differ from those depicted in Figure 10.3, we, first, apply the above algorithm (with R and S taken from the analysis of observations presented in Figure 10.3) to determine G and J under stretching, and afterwards, employ the same technique to find parameters K, R, S under retraction. The best-fit value $K = 150.0$

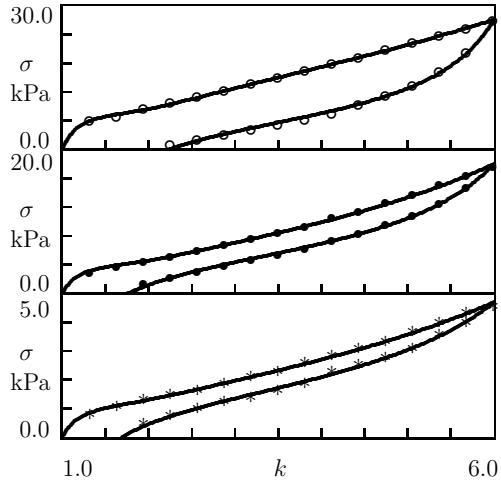

Figure 10.8 Stress σ versus elongation ratio k. Symbols: experimental data in cyclic tests on DMAA-Si hydrogels with $\phi_{\rm p} = 142$ g/L and various $\phi_{\rm f}$ g/L ($\circ$ – 710.5; $\bullet$ – 284.4; $*$ – 142.7). Solid lines: results of simulation.

is found by matching observations on hydrogel with $\phi_{\rm f} = 710.5$ g/L and used without changes to approximate observations on other specimens. Numerical analysis shows that the best-fit values of J are slightly lower and the best-fit values of G are slightly higher than those found by matching observations in Figure 10.3.

The effect of concentration of solid phase $\phi_{\rm s}$ on coefficients $\tilde{G}$ and S found by matching observations under retraction is illustrated in Figure 10.9. The data are approximated by the equations

$$\log \tilde{G} = \tilde{G}_0 - \tilde{G}_1 \phi_{\rm s}, \qquad \log S = S_0 + S_1 \phi_{\rm s}, \tag{10.71}$$

with coefficients calculated by the least-squares method. Figure 10.9 shows that the energy of inter-chain interactions $\tilde{G}$ decreases and rate of plastic deformation S increases with concentration of solid phase.

To examine the kinetics of plastic flow under cyclic loading, integration of the stress–strain relations is conducted with the adjustable parameters found by matching observations in Figure 10.8. Results of simulation are presented in Figure 10.10. The following conclusions are drawn: (i) under tension, plastic elongation ratio $k_{\rm p}$ increases monotonically with k and remains practically independent of clay content (in agreement with the data reported in Figure 10.5), (ii) under retraction, $k_{\rm p}$ grows pronouncedly at the initial

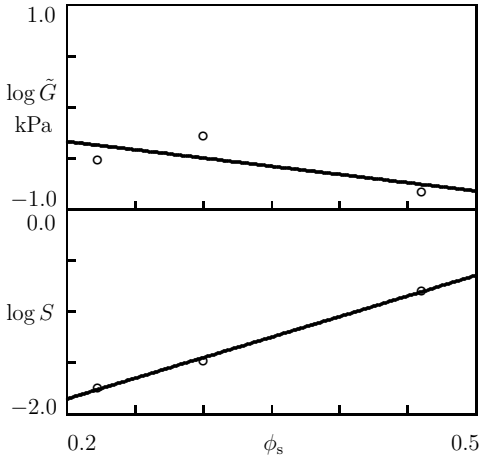

Figure 10.9 Parameters $\tilde{G}$ and S versus concentration of solid phase ϕ_s. Circles: treatment of observations under retraction in cyclic tests on DMAA-Si hydrogels with $\phi_p = 142$ g/L and various ϕ_f g/L. Solid lines: approximation of the data by Equation (10.71).

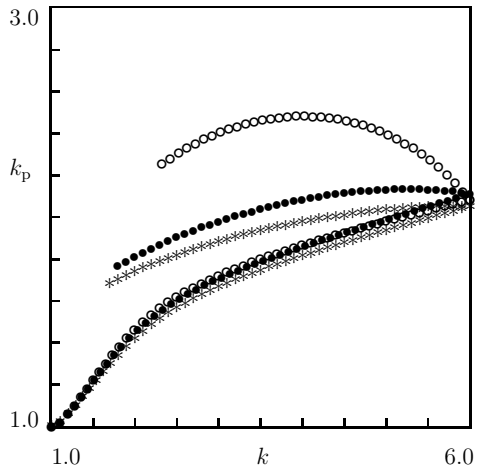

Figure 10.10 Elongation ratio for plastic deformation k_p versus elongation ratio k. Symbols: results of simulation for cyclic tests on DMAA-Si hydrogels with $\phi_p = 142$ g/L and various ϕ_f g/L (○ – 710.5; ● – 284.4; ∗ – 142.7).

stage of unloading (when k remains in the vicinity of k_{max}), reaches its maximum (plastic overshoot), and decreases afterwards, (iii) intensity of plastic overshoot ($k_{p\,max}$) and residual strain (k_p at the instant when σ vanishes) increase strongly (by twice) with nanoclay content.

10.4.3 As-Prepared Polyacrylamide–Clay Hydrogels

To verify the above conclusions regarding the influence of strain rate and nanofiller content on the viscoplastic response of nanocomposite hydrogels, experimental data are approximated on polyacrylamide–nanoclay (PAM-NC) hydrogels manufactured by free-radical polymerization of acrylamide (AM) monomers in aqueous suspensions of hectorite nanoclay (NC) Laponite RD by using KPS and TEMED as initiator and catalyst, respectively [42].

First, we approximate observations on as-prepared samples with various concentrations of polymer network $\phi_{\rm p}$ and filler $\phi_{\rm f}$ in tensile tests with strain rates $\dot{\epsilon} = 0.083, 0.83,$ and $1.67\ s^{-1}$ at room temperature. Experimental data are presented in Figures 11–13 for nanocomposite hydrogels with $\phi_{\rm p} = 200$ g/L, $\phi_{\rm f} = 20$ g/L, $\phi_{\rm p} = 250$ g/L, $\phi_{\rm f} = 20$ g/L, and $\phi_{\rm p} = 100$ g/L, $\phi_{\rm f} = 40$ g/L.

For each concentration of polymer and filler, we start with matching observations under tension with the highest strain rate $\dot{\epsilon} = 1.67\ s^{-1}$, and determine parameters G, J, R, S by means of the above algorithm. Afterwards, we fix the best-fit value of J and approximate the other stress–strain diagrams with the help of three parameters G, S, R.

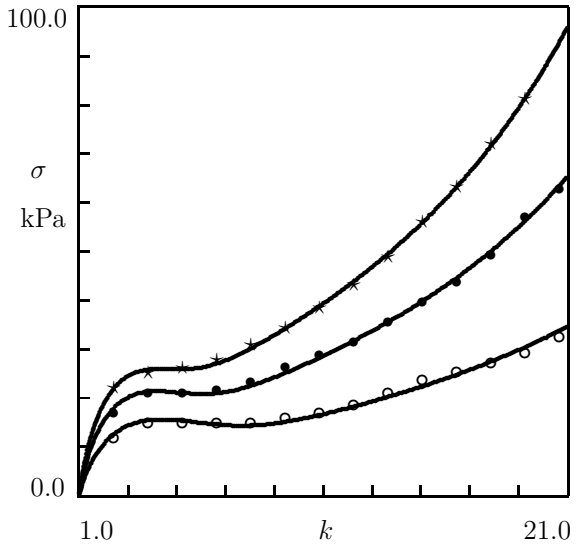

Figure 10.11 Stress σ versus elongation ratio k. Symbols: observations in tensile tests with various strain rates $\dot{\epsilon}$ s^{-1} on PAM-NC hydrogels with $\phi_{\rm p} = 200$ g/L and $\phi_{\rm f} = 20$ g/L ($\circ - \dot{\epsilon} = 0.083$; $\bullet - \dot{\epsilon} = 0.83$; $\star - \dot{\epsilon} = 1.67$). Solid lines: results of simulation.

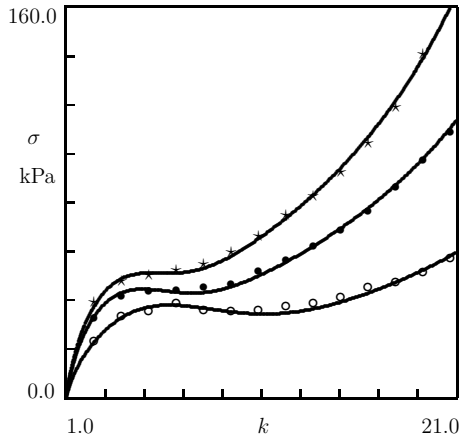

Figure 10.12 Stress σ versus elongation ratio k. Symbols: observations in tensile tests with various strain rates $\dot{\epsilon}$ s^{-1} on PAM-NC hydrogel with $\phi_p = 250$ g/L and $\phi_f = 20$ g/L ($\circ - \dot{\epsilon} = 0.083$; $\bullet - \dot{\epsilon} = 0.83$; $\star - \dot{\epsilon} = 1.67$). Solid lines: results of simulation.

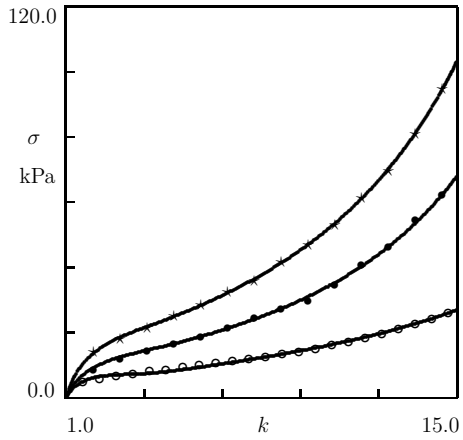

Figure 10.13 Stress σ versus elongation ratio k. Symbols: observations in tensile tests with various strain rates $\dot{\epsilon}$ s^{-1} on PAM-NC hydrogel with $\phi_p = 100$ g/L and $\phi_f = 40$ g/L ($\circ - \dot{\epsilon} = 0.083$; $\bullet - \dot{\epsilon} = 0.83$; $\star - \dot{\epsilon} = 1.67$). Solid lines: results of simulation.

The effect of strain rate $\dot{\epsilon}$ on elastic modulus G is illustrated in Figure 10.14 where G is plotted versus duration of loading $t' = (k_{max} - 1)/\dot{\epsilon}$. For comparison, experimental data in shear relaxation tests with small strain $\epsilon = 0.005$ are also presented (as observations in relaxation tests on specimens with $\phi_p = 200$ g/L, $\phi_f = 20$ g/L were not reported in [42], we replace

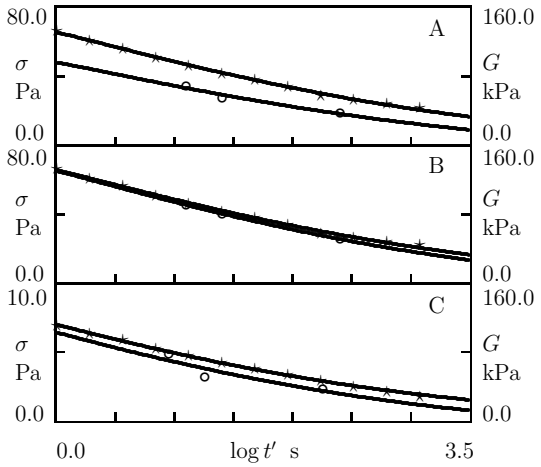

Figure 10.14 Dimensionless stress $\tilde{\sigma}$ ($\star$) versus relaxation time t' and modulus G versus loading time t'. Symbols: observations on PAM-NC hydrogels with $\phi_{\rm p} = 200$ g/L, $\phi_{\rm f} = 20$ g/L (A), $\phi_{\rm p} = 250$ g/L, $\phi_{\rm f} = 20$ g/L (B), $\phi_{\rm p} = 100$ g/L, $\phi_{\rm f} = 40$ g/L (C). Stars: experimental data in tensile relaxation test with strain $\epsilon = 0.005$. Circles: treatment of experimental data in tensile tests with various strain rates. Solid lines: results of simulation.

them with those on samples with $\phi_{\rm p} = 250$ g/L, $\phi_{\rm f} = 20$ g/L). According to Figure 10.14, an increase in elastic modulus with strain rate revealed by fitting observations in tensile tests may be attributed to the viscoelastic response of hydrogels (in agreement with the conclusion drawn from Figure 10.7).

To assess the influence of strain rate on the viscoplastic flow, parameter S is plotted versus $\dot{\epsilon}$ in Figure 10.15. The data are approximated by the equation

$$\log S = S_0 + S_1 \log \dot{\epsilon}, \tag{10.72}$$

where the coefficients are calculated by the least-squares technique. Equation (10.72) demonstrates that S increases monotonically with $\dot{\epsilon}$, but the rate of growth is strongly sub-linear: $S \sim \dot{\epsilon}^{\beta}$ with $\beta \approx 0.2$.

Given G and R, we calculate $\tilde{G}$ from Equation (10.67) and plot this quantity versus strain rate $\dot{\epsilon}$ in Figure 10.16. The data are approximated by the equation

$$\log \tilde{G} = \tilde{G}_0 + \tilde{G}_1 \log \dot{\epsilon} \tag{10.73}$$

with coefficients calculated by the least-squares technique. Figure 10.16 demonstrates a pronounced difference between PAM-NC hydrogels (for which $\tilde{G}$ increases strongly with strain rate) and DMAA-Si hydrogels (for which this parameter is independent of $\dot{\epsilon}$).

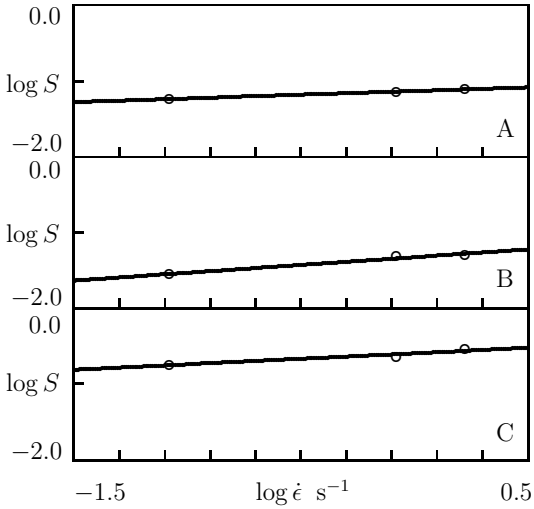

Figure 10.15 Parameter S versus strain rate $\dot{\epsilon}$. Circles: treatment of observations in tensile tests on PAM-NC hydrogels with $\phi_{\mathrm{p}} = 200$ g/L, $\phi_{\mathrm{f}} = 20$ g/L (A), $\phi_{\mathrm{p}} = 250$ g/L, $\phi_{\mathrm{f}} = 20$ g/L (B), $\phi_{\mathrm{p}} = 100$ g/L, $\phi_{\mathrm{f}} = 40$ g/L (C). Solid lines: approximation of the data by Equation (10.72).

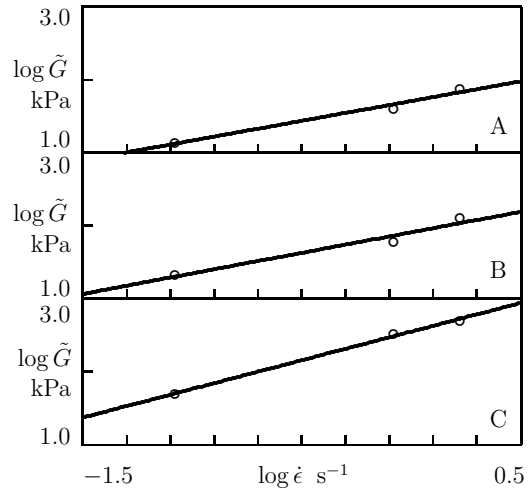

Figure 10.16 Parameter $\tilde{G}$ versus strain rate $\dot{\epsilon}$. Circles: treatment of observations in tensile tests on PAM-NC hydrogels with $\phi_{\mathrm{p}} = 200$ g/L, $\phi_{\mathrm{f}} = 20$ g/L (A), $\phi_{\mathrm{p}} = 250$ g/L, $\phi_{\mathrm{f}} = 20$ g/L (B), $\phi_{\mathrm{p}} = 100$ g/L, $\phi_{\mathrm{f}} = 40$ g/L (C). Solid lines: approximation of the data by Equation (10.73).

To examine the effect of concentration of solid phase $\phi_{\rm s}$ on the mechanical response of nanocomposite hydrogels under cyclic loading, we approximate stress–strain curves under tension with constant strain rate $\dot{\epsilon} = 0.083\ {\rm s}^{-1}$ up to maximum elongation ratio $k_{\max} = 17$ followed by retraction with the same strain rate down to the zero minimum stress $\sigma_{\min} = 0$. Observations on specimens with $\phi_{\rm f} = 20$ g/L, $\phi_{\rm p} = 200$ and 250 g/L are reported in Figure 10.17, and those on samples with $\phi_{\rm p} = 100$ g/L, $\phi_{\rm f} = 30$ and 40 g/L are presented in Figure 10.18 together with results of simulation. Adjustable parameters in the stress–strain relations are found by fitting each set of data separately by means of the same algorithm that was employed to match observations in Figure 10.8. As the stress–strain diagrams under tension in Figures 10.17, 10.18 differ from those reported in Figures 10.11–10.13, they are approximated by using four parameters G, J, S, R. Afterwards, unloading paths of the stress–strain curves are fitted with the help of three coefficients K, S, R.

Adjustable parameters determined by matching observations under tension and retraction are reported in Figures 10.19, 10.20, where they are plotted versus concentration of solid phase $\phi_{\rm s}$. The data are approximated by the equations

$$\log G = G_0 + G_1\phi_{\rm s}, \qquad \log \tilde{G} = \tilde{G}_0 + \tilde{G}_1\phi_{\rm s}, \qquad \log S = S_0 + S_1\phi_{\rm s},$$

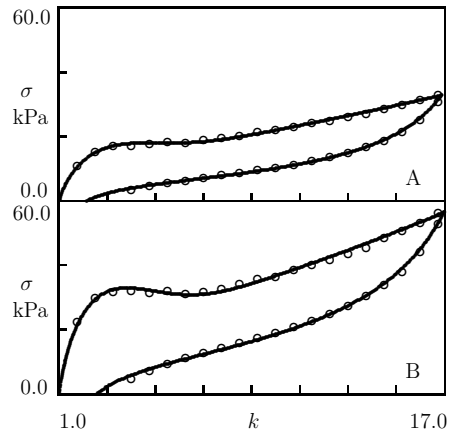

Figure 10.17 Stress σ versus elongation ratio k. Circles: experimental data in cyclic tensile tests on PAM-NC hydrogels with $\phi_{\rm f} = 20$ g/L and $\phi_{\rm p} = 200$ g/L (A), $\phi_{\rm p} = 250$ g/L (B). Solid lines: results of simulation.

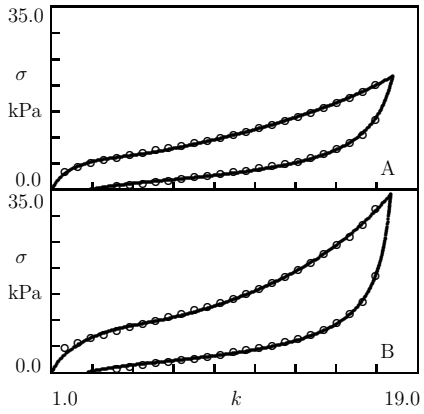

Figure 10.18 Stress σ versus elongation ratio k. Circles: experimental data in cyclic tests on PAM-NC hydrogels with $\phi_{\rm n} = 100$ g/L and $\phi_{\rm f} = 30$ g/L (A), $\phi_{\rm f} = 40$ g/L (B). Solid lines: results of simulation.

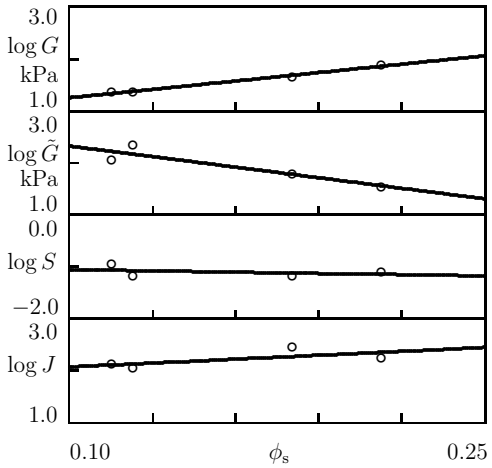

Figure 10.19 Parameters $G, \tilde{G}, S, J$ versus concentration of solid phase $\phi_{\rm s}$. Circles: treatment of observations under tension in cyclic tests on PAM-NC hydrogels. Solid lines: approximation of the data by Equation (10.74).

$$\log J = J_0 + J_1\phi_{\rm s} \tag{10.74}$$

under tension and

$$\log \tilde{G} = \tilde{G}_0 + \tilde{G}_1\phi_{\rm s}, \qquad \log S = S_0 + S_1\phi_{\rm s}, \qquad \log K = K_0 + K_1\phi_{\rm s} \tag{10.75}$$

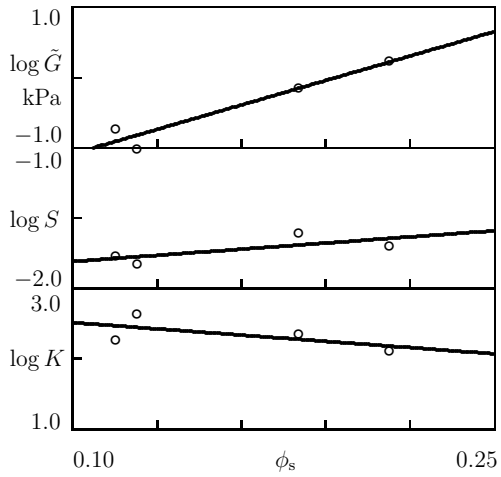

Figure 10.20 Parameters $\tilde{G}, S, K$ versus concentration of solid phase ϕ_s. Circles: treatment of observations under retraction in cyclic tests on PAM-NC hydrogels. Solid lines: approximation of the data by Equation (10.75).

under retraction. The coefficients in Equations (10.74), (10.75) are calculated by the least-squares method.

To examine how concentrations of polymer and filler, ϕ_p and ϕ_f, affect plastic flow in PAM-NC hydrogels under cyclic deformations, numerical integration of the stress–strain relations is performed for cyclic loading with strain rate $\dot{\epsilon} = 0.083\ s^{-1}$, maximum elongation ratio under stretching $k_{max} = 17$, and the zero minimum stress under retraction. Results of simulation are reported in Figure 10.21. The following conclusions are drawn: (i) the dependency $k_p(k)$ for PAM-NC hydrogels is qualitatively similar to that for DMAA-Si hydrogels (elongation ratio for plastic deformation increases under tension and reveals a pronounced overshoot under retraction), (ii) given ϕ_f, an increase in polymer concentration ϕ_p results in a modest increase in k_p under tension and retraction, whereas (iii) given ϕ_p, an increase in nanoclay concentration ϕ_f induces a decay in plastic deformation.

10.4.4 Discussion

Figures 10.1, 10.3, 10.6, 10.11–10.13 demonstrate ability of the constitutive model with four adjustable parameters G, J, R, S to describe stress–strain diagrams under uniaxial tension with finite deformations (elongation ratios up to 20).

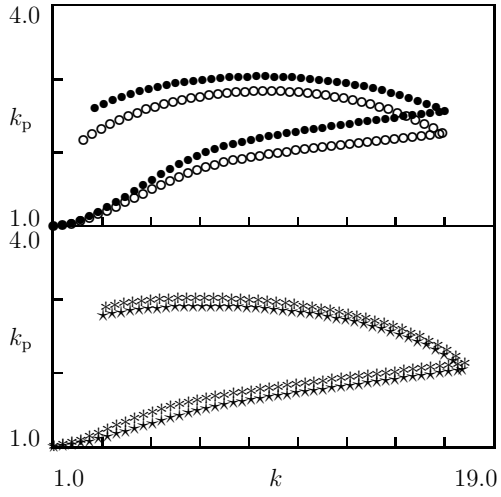

Figure 10.21 Elongation ratio for plastic deformation $k_{\rm p}$ versus elongation ratio k. Symbols: results of simulation for cyclic tests on PAM-NC hydrogels ($\circ$ – $\phi_{\rm p} = 200$ g/L, $\phi_{\rm f} = 20$ g/L; $\bullet$ – $\phi_{\rm p} = 250$ g/L, $\phi_{\rm f} = 20$ g/L; $*$ – $\phi_{\rm p} = 100$ g/L, $\phi_{\rm f} = 30$ g/L; $\star$ – $\phi_{\rm p} = 100$ g/L, $\phi_{\rm f} = 40$ g/L).

Figures 10.8, 10.17, 10.18 show good agreement between observations in cyclic (loading–unloading) tests and results of simulation based on the constitutive equations that involve three additional parameters for retraction R, S, and K.

According to Figures 10.4, 10.9, 10.19, 10.20, phenomenological Equations (10.70), (10.71), (10.74), (10.75) describe correctly evolution of adjustable parameters with concentration of solid phase (which means that $\phi_{\rm s}$ may serve as the only parameter characterizing mechanical properties of nanocomposite hydrogels).

Figures 10.15, 10.16 reveal that Equations (10.72), (10.73) predict adequately the effect of strain rate $\dot{\epsilon}$ on parameters $\tilde{G}$ and S.

An advantage of the constitutive equations is that they involve a relatively small number of material constants, on the one hand, and describe correctly experimental data in cyclic tensile tests, on the other. A shortcoming of the model is that it disregards viscoelastic properties of nanocomposite hydrogels. As a result, the elastic modulus is allowed to alter with strain rate in the fitting procedure. Although these changes are confirmed by comparison with observations in relaxation tests (Figures 10.7 and 10.14), they restrict applicability of the model to deformation processes with constant strain rates. To describe

time-dependent phenomena in nanocomposite hydrogels, rearrangement of the networks of flexible chains and nanoparticles should be modeled explicitly (the latter leads, however, to a noticeable increase in the number of material constants).

Comparison of experimental data under cyclic deformation with results of numerical simulation demonstrates that elongation ratio for plastic deformation k_{p} grows monotonically under tension and reveals a non-monotonic behavior under retraction: k_{p} increases, reaches its maximum value (plastic overshoot), and decreases afterwards (Figures 10.10 and 10.21). Intensity of the overshoot increases with concentration of solid phase, but the rate of its growth depends strongly on type of nanofiller.

10.5 Concluding Remarks

A constitutive model is developed in finite viscoplasticity of nanocomposite hydrogels under an arbitrary deformation with finite strains. A hydrogel is treated as a two-phase medium composed of a solid phase (polymer network reinforced with nanoparticles) and a fluid phase (solvent). Transport of solvent through a hydrogel is treated as its diffusion governed by the gradient of chemical potential.

Constitutive equations are derived by means of the free-energy imbalance equation. The free energy of a nanocomposite hydrogel equals the sum of strain energy density of the solid phase and the energy of mixing of the solid phase with solvent.

The solid phase is modeled as an isotropic compressible viscoplastic medium, whose deformation gradient is split into the product of deformation gradients for elastic deformation, plastic deformation, and deformation induced by swelling (characterized by the coefficient of inflation of the polymer network). Strain energy density of the solid phase equals the sum of the stored mechanical energy and the energy of interaction between chains and nanoparticles.

The constitutive equations involve (i) stress–strain relation, (ii) flow rule for plastic deformation, and (iii) diffusion equation for solvent. These relations are accompanied by equations for mechanical equilibrium and appropriate boundary conditions.

The model is applied to the analysis of rapid deformation (the rate of loading exceeds strongly the rate of solvent diffusion) of (i) nanocomposite hydrogels subjected to drying and subsequent re-swelling, and (ii) as-prepared nanocomposite hydrogels.

Analysis of observations in uniaxial tensile tests on nanocomposite hydrogels subjected to drying and reswelling demonstrates that the constitutive equations describe adequately the effect of rearrangement of the secondary network of clay platelets under drying on the mechanical response of reswollen gels (Figure 10.1). The effect of drying–reswelling can be accounted for with the help of the only parameter that changes consistently with solvent content (Figure 10.2).

Approximation of observations in uniaxial tensile tests and tensile cyclic tests on as-prepared nanocomposite hydrogels reinforced with Si particles and clay platelets shows that the constitutive equations with four adjustable parameters under stretching and three more parameters under retraction describe correctly the experimental stress–strain diagrams and predict characteristic features of plastic flow (in particular, plastic overshoot under retraction).

10.6 Acknowledgement

Financial support by the EU Commission through Project Evolution-314744 is gratefully acknowledged.

References

[1] Naficy, S., Brown, H.R., Razal, J.M., Spinks, G.M., Whitten, P.G., 'Progress toward robust polymer hydrogels', Australian J. Chem., 64, 1007–1025, 2011.

[2] Haque, M.A., Kurokawa, T., Kamita, G., Gong, J.P., 'Lamellar bilayers as reversible sacrificial bonds to toughen hydrogel: hysteresis, self-recovery, fatigue resistance, and crack blunting', Macromolecules, 44, 8916–8924, 2011.

[3] Schexnailder P., Schmidt, G., 'Nanocomposite polymer hydrogels', Colloid Polym. Sci., 287, 1–11, 2009.

[4] Haraguchi, K., 'Stimuli-responsive nanocomposite gels', Colloid Polym. Sci., 289, 455–473, 2011.

[5] Deligkaris, K., Tadele, T.S., Olthuis, W., van den Berg, A., 'Hydrogel-based devices for biomedical applications', Sensors Actuators B, 147, 765–774, 2010.

[6] Messing, R., Schmidt, A.M., 'Perspectives for the mechanical manipulation of hybrid hydrogels', Polym. Chem., 2, 18–32, 2011.

[7] Buenger, D., Topuz, F., Groll, J., 'Hydrogels in sensing applications', Progr. Polym. Sci., 37, 1678–1719, 2012.
[8] Qian, Z.-Y., Fu, S.-Z., Feng, S.-S., 'Nanohydrogels as a prospective member of the nanomedicine family', Nanomedicine, 8, 161–164, 2013.
[9] Higuchi, A., Ling, Q.-D., Chang, Y., Hsu, S.-T., Umezawa, A., 'Physical cues of biomaterials guide stem cell differentiation fate', Chem. Rev., 113, 3297–3328, 2013.
[10] Discher, D.E., Mooney, D.J., Zandstra, P.W., 'Growth factors, matrices, and forces combine and control stem cells', Science, 324, 1673–1677, 2009.
[11] Song, M.J., Dean, D., Knothe Tate, M.L., 'Mechanical modulation of nascent stem cell lineage commitment in tissue engineering scaffolds', Biomaterials, 34, 5766–5775, 2013.
[12] Pelaez, D., Huang, C.-Y.C, Cheung, H.S., 'Cyclic compression maintains viability and induces chondrogenesis of human mesenchymal stem cells in fibrin gel scaffolds', Stem Cells Develop., 18, 93–102, 2009.
[13] Meyer, E.G., Buckley, C.T., Steward, A.J., Kelly, D.J., 'The effect of cyclic hydrostatic pressure on the functional development of cartilaginous tissues engineered using bone marrow derived mesenchymal stem cells', J. Mech. Behav. Biomed. Mater., 4, 1257–1265, 2011.
[14] Hong, W., Zhao, X., Zhou, J., Suo, Z., 'A theory of coupled diffusion and large deformation in polymeric gels', J. Mech. Phys. Solids, 56, 1779–1793, 2008.
[15] Hong, W., Liu, Z., Suo, Z., 'Inhomogeneous swelling of a gel in equilibrium with a solvent and mechanical load', Int. J. Solids Struct., 46, 3282–3289, 2009.
[16] Duda, F.P., Souza, A.C., Fried, E., 'A theory for species migration in finitely strained solid with application to polymer network swelling', J. Mech. Phys. Solids, 58, 515–529, 2010.
[17] Chester, S.A., Anand, L., 'A coupled theory of fluid permeation and large deformations for elastomeric materials', J. Mech. Phys. Solids, 58, 1879–1906, 2010.
[18] Baek, S., Pence, T.J., 'Inhomogeneous deformation of elastomer gels in equilibrium under saturated and unsaturated conditions', J. Mech. Phys. Solids, 59, 561–582, 2011.
[19] Yan, H., Jin, B., 'Influence of microstructural parameters on mechanical behavior of polymer gels', Int. J. Solids Struct., 49, 436–444, 2012.

[20] Drozdov, A.D., Christiansen, J.deC., 'Constitutive equations in finite elasticity of swollen elastomers', Int. J. Solids Struct., 50, 1494–1504, 2013.
[21] Drozdov, A.D., Christiansen, J.deC., 'Stress–strain relations for hydrogels under multiaxial deformation', Int. J. Solids Struct., 50, 3570–3585, 2013.
[22] Lucantonio, A., Nardinocchi, P., Teresi, L., 'Transient analysis of swelling-induced large deformations in polymer gels', J. Mech. Phys. Solids, 61, 205–218, 2013.
[23] Zhao, X., Huebsch, N., Mooney, D.J., Suo, Z., 'Stress–relaxation behavior in gels with ionic and covalent crosslinks', J. Appl. Phys., 107, 063509, 2010.
[24] Chester, S.A., 'A constitutive model for coupled fluid permeation and large viscoelastic deformation in polymeric gels', Soft Matter, 8, 8223–8233, 2012.
[25] Wang, X., Hong, W., 'A visco-poroelastic theory of polymeric gels', Proc. Roy. Soc. A, 468, 3824–3841, 2012.
[26] Strange, D.G.T., Fletcher, T.L., Tonsomboon, K., Brawn, H., Zhao, X., Oyen, M.L., 'Separating poroviscoelastic deformation mechanisms in hydrogels', Appl. Phys. Lett., 102, 031913, 2013.
[27] Baumberger, T., Caroli, C., Martina, D., 'Solvent control of crack dynamics in a reversible hydrogel', Nature Mater., 5, 552–555, 2006.
[28] Seitz, M.E., Martina, D., Baumberger, T., Krishnan, V.R., Hui, C.-Y., Shull, K.R., 'Fracture and large strain behavior of self-assembled triblock copolymer gels', Soft Matter, 5, 447–456, 2009.
[29] Kundu, S., Crosby, A.J., 'Cavitation and fracture behavior of polyacrylamide hydrogels', Soft Matter, 5, 3963–3968, 2009.
[30] Wang, X., Hong, W., 'Delayed fracture in gels', Soft Matter, 8, 8171–8178, 2012.
[31] Zhang, J., An, Y., Yazzie, K., Chawla, N., Jiang, H., 'Finite element simulation of swelling-induced crack healing in gels', Soft Matter, 8, 8107–8112, 2012.
[32] Korchagin, V., Dowbow, J., Stepp, D., 'A theory of amorphous viscoelastic solids undergoing finite deformations with application to hydrogels', Int. J. Solids Struct., 44, 3973–3997, 2007.
[33] Wang, X., Hong, W., 'Pseudo-elasticity of a double network gel', Soft Matter, 7, 8576–8581, 2011.
[34] Zhao, X., 'A theory for large deformation and damage of interpenetrating polymer networks', J. Mech. Phys. Solids, 60, 319–332, 2012.

[35] Haraguchi, K., Li, H.-J., 'Mechanical properties and structure of polymer–clay nanocomposite gels with high clay content', Macromolecules, 39, 1989–1905, 2006.
[36] Bakarich, S.E., Pidcock, G.C., Balding, P., Stevens, L., Calvert, P., in het Panhuis, M., 'Recovery from applied strain in interpenetrating polymer network hydrogels with ionic and covalent cross-links', Soft Matter, 8, 9985–9988, 2012.
[37] Gent, A.N., 'A new constitutive relation for rubber', Rubber Chem. Technol., 69, 59–61, 1996.
[38] Wall, F.T., Flory, P.J., 'Statistical thermodynamics of rubber elasticity', J. Chem. Phys., 19, 1435–1439, 1951.
[39] Haraguchi, K., Li, H.-J., Ren, H.-J., Zhu, M., 'Modification of nanocomposite gels by irreversible rearrangement of polymer/clay network structure through drying', Macromolecules, 43, 9848–9853, 2010.
[40] Carlsson, L., Rose, S., Hourdet, D., Marcellan, A., 'Nano-hybrid self-crosslinked PDMA/ silica hydrogels', Soft Matter, 6, 3619–3631, 2010.
[41] Drozdov, A.D., Christiansen, J.deC., 'Thermo-viscoelastic and viscoplastic behavior of high-density polyethylene', Int. J. Solids Struct., 45, 4274–4288, 2008.
[42] Xiong, L., Hu, X., Liu, X., Tong, Z., 'Network chain density and relaxation of in situ synthesized polyacrylamide/hectorite clay nanocomposite hydrogels with ultrahigh tensibility', Polymer, 49, 5064–5071, 2008.